



Step-by-step challenge of debris characterization for the decommissioning of Fukushima-Daiichi Nuclear Power Station (FDNPS)

Masaki Kurata, Naoaki Okuzumi, Akira Nakayoshi, Hiroto Ikehuchi & Shinichi Koyama

To cite this article: Masaki Kurata, Naoaki Okuzumi, Akira Nakayoshi, Hiroto Ikehuchi & Shinichi Koyama (2022): Step-by-step challenge of debris characterization for the decommissioning of Fukushima-Daiichi Nuclear Power Station (FDNPS), Journal of Nuclear Science and Technology, DOI: [10.1080/00223131.2022.2040393](https://doi.org/10.1080/00223131.2022.2040393)

To link to this article: <https://doi.org/10.1080/00223131.2022.2040393>

 View supplementary material [↗](#)

 Published online: 10 Apr 2022.

 Submit your article to this journal [↗](#)

 Article views: 132

 View related articles [↗](#)

 View Crossmark data [↗](#)

Step-by-step challenge of debris characterization for the decommissioning of Fukushima-Daiichi Nuclear Power Station (FDNPS)

Masaki Kurata^{a,b}, Naoaki Okuzumi^b, Akira Nakayoshi^{a,b}, Hiroto Ikehata^{a,b} and Shinichi Koyama^{a,b}

^aJapan Atomic Energy Agency (JAEA), Collaborative Laboratories for Advanced Decommissioning Science (CLADS), Motooka-Otsuka, Tomioka-machi, Fukushima-ken, Japan; ^bInternational Research Institute for Nuclear Decommissioning (Irid), Nishi-Shinbashi, Minato-ku, Tokyo, Japan

Abstract

The present article reviewed the step-by-step attempts on debris characterization after the severe accident of Fukushima-Daiichi Nuclear Power Station (FDNPS). It was rather difficult to investigate the reactor inside in the first few years. Distribution of degraded core materials, i.e. fuel debris, was investigated by a muon tomography and the damaged reactor status was preliminarily predicted from the severe accident analysis. In parallel, literature review was carried out for the debris generated after Three Mile Island unit 2 accident and the simulated debris previously examined in the nuclear safety research. Since 2017, remote investigations of the reactor inside have been carried out, which is gradually clarifying the damage status. The sample analysis has accumulated useful knowledge for the debris characterization. Furthermore, several out-of-pile tests which reflected unique accident conditions at the FDNPS have been conducted mainly in Japan, including characterization of simulated ex-vessel debris, formation mechanism of metal-rich debris and debris corrosion by seawater materials. To establish a proper analysis method suitable for debris samples is also extremely important. These accumulated knowledge and data have been reviewed and compiled as a database 'debrisWiki' in Japan, which includes core status maps, investigation results of the reactor inside, probable accident scenarios, sample analysis data and so on. Various international collaborations were launched and several have continued for the decommissioning of the FDNPS and the use of relevant knowledge for improving the nuclear safety.

ARTICLE HISTORY

Received 30 September 2021
Accepted 1 February 2022

KEYWORDS

Fukushima Daiichi Nuclear Power Station; severe accident; PCV inside investigation; fuel debris; corium; core status; FDNPS samples

1. Introduction

The Great East Japan Earthquake occurred at 14:46 (Japan time zone) on 11 March 2011. At the time of the earthquake, Unit 1, Unit 2 and Unit 3 operating at Tokyo Electric Power Corporation (TEPCO) Fukushima Daiichi Nuclear Power Station (hereinafter referred to as 'FDNPS') were properly shut down. Following the earthquake, a huge tsunami attacked the FDNPS site, resulting in a total or partial loss of core cooling capability due to the loss of total DC power. The cooling water could not be sufficiently supplied to the cores, and then the cores were gradually exposed to steam atmosphere. As a result, the three cores were significantly degraded and slumped down (so-called 'melt down'). In the meantime, certain amounts of hydrogen were generated by the steam oxidation of zirconium (the major component of fuel-cladding and channel box) and accumulated in the reactor buildings (R/B). Then, hydrogen explosions happened in Unit 1 and Unit 3 that severely damaged the R/B. The R/B of Unit 4 was also severely damaged by the hydrogen explosion

(presumably caused by the hydrogen flowing in from Unit 3). Consequently, the 'confinement' function was lost and a significant amount of radioactive materials was released to the environment atmosphere. Furthermore, the barrier of the Reactor Pressure Vessel (RPV) was severely damaged by the molten core materials (so-called 'corium'), which slumped down from the core region. Then, a significant amount of corium spread out of the RPV (so-called 'melt through'). These sequences could likely form 'in-vessel' debris (the RPV inside) and 'ex-vessel' debris (the RPV outside), respectively. Emergency water injection using seawater was temporarily attempted by fire engines to cool the inside of the RPV for several days after the tsunami attack.

After that, a circulating water injection cooling system was introduced adjacent to the severely damaged R/B that is able to remove radioactive substances from the contaminated cooling water and recycle the treated water into the Primary Containment Vessel (PCV) via the RPV for continuous cooling. In December 2011, the temperature at the bottom of the RPV fell below approximately 100°C

and the release of radioactive materials was significantly suppressed and controlled. Due to these facts, the Nuclear Emergency Response Headquarters (NERH) of the Japanese Government has decided that these severely damaged units have reached 'a cold shutdown' [1].

An expert group of mid- to long-term measures for TEPCO FDNPS decommissioning, which was established by Japan Atomic Energy Commission (JAEC) in August 2011, organized and categorized the relevant technical issues and R&D items necessary for the decommissioning of Units 1 to 4. Then, referring to the report of JAEC, in November 2011, Minister of the Economy, Trade and Industry (METI) and Minister for the Restoration from and Prevention of Nuclear Accident (MRPNA) co-instructed three organizations; TEPCO, Agency for Natural Resources and Energy (ANRE), and Nuclear and Industrial Safety Agency (NISA, at that time); to formulate a mid- and long-term roadmap for the FDNPS decommissioning. Consequently, on 21 December 2011 the Japanese Government and TEPCO Council on Mid-to-Long-Term Response for Decommissioning established within the NERH decided and published the first edition of the Mid-and-Long-Term Roadmap [2], in which the period for decommissioning is divided into three phases:

- [Phase 1 (SFP fuel removal)] commencing with fuel removal from the spent fuel pools;
- [Phase 2 (examination & preparation of damaged units)] starting with the completion of Phase 1 to the commencement of the fuel debris removal from the first unit;
- [Phase 3 (fuel debris removal & clean-up)] starting from the completion of Phase 2 to the completion of the decommissioning.

The roadmap as indicated in [2] also proposed concepts for the debris retrieval in the near future in 2017:

- Step-by-step approach, starting from a small amount and then gradually to a larger scale;
- Optimization of the entire process, including preparatory work, construction of access route, debris retrieval, handling, storage, waste management and clean up;
- Combination of multiple methods, according to the existing regions of debris, e.g. horizontal access to the bottom region of the PCV and top access to the inside of the RPV;
- Focusing on the fuel debris retrieval in the air (not submerged in water and by maintaining non-oxidizing atmosphere);

- Preceding the debris retrieval by horizontal access to the inside of the RPV.

Current status is recognized as being at the end of Phase 2, in which the first debris retrieval is on schedule (planned by the end of 2022) from the RPV pedestal of Unit 2. The knowledge regarding the debris characteristics, amount and distribution and the status of damaged reactors were essential for the relevant decisions.

Although the information at the FDNPS on-site was rather limited for the first few years after accident (especially, the inside of the RPV has not been investigated yet), various investigations have been attempted to understand the status of damaged reactors. The most important issues were to identify the distribution and amount of degraded core materials, so-called 'fuel debris' [3], and to confirm the integrity of the PCV. Cosmic-ray muons that can penetrate these severely damaged reactors were used to detect the approximate locations of high-density materials (including nuclear fuels), by a muon tomography technique. The results indicated that the high-density materials hardly remained in the RPV of Unit 1 and Unit 3, and whereas a significant amount of the high-density materials was detected in the lower part of the RPV of Unit 2. Since JFY2017 (Japanese Financial Year), the remote investigations of the inside of the PCV have continued using the various types of robot, each of which was originally designed for the individual conditions of one unit. Step by step attempts using these robots enable the status of the inside of the PCV to be clarified, in particular, on the damage to structural and internal materials and the accumulation of fuel debris. Several small samples were taken via these interior inspections, including the smear samples taken from the investigation robots and the obstacle samples taken during the routes of these robots. Hereafter, these samples are referred to as 'FDNPS samples.' The analysis of these samples is ongoing in the hot cells in Ibaraki prefecture in Japan under several projects of Decommissioning and Contaminated Water management [4], which have been coordinated by the International Research Institute for Nuclear Decommissioning (IRID) [5]. In the present review, the chronicle of the PCV inside investigation and the major findings from the FDNPS sample analysis are outlined in Chapters 2 and 3, respectively.

Despite these attempts above, it was rather difficult to understand the characteristics of the accumulated fuel debris generated in the three units of the FDNPS.

Hence, JAEA has attempted literature review of the Three Mile Island Unit 2 (TMI-2) accident and in parallel of the relevant knowledge for various simulated debris previously examined in nuclear safety research. However, the knowledge was mostly relevant to the in-vessel phenomena for the prototypical accident sequences of Pressurized Water Reactor (PWR). Regarding the accident sequences and debris characteristics for Boiling Water Reactor (BWR) in particular as for the ex-vessel debris, the information was not sufficient. Also, the corrosion of fuel debris by seawater materials was pointed out as a unique concern in characterizing the FDNPS debris. Therefore, several out-of-pile tests using surrogate materials, so-called ‘sim-debris,’ that reflected the accident conditions of the FDNPS were conducted mainly in Japan by JAEA. The major findings of these studies are outlined in Chapter 4. To establish a proper analysis method suitable for the debris sample is also extremely important in the early stage of the decommissioning. The current progress on the development of debris analysis method is also introduced in Chapter 4.

Various international collaborations had been launched and several have continued for the decommissioning of the FDNPS and the use of the FDNPS knowledge for the improvement of nuclear safety. In Chapter 5, the major R&D projects directly relevant to the FDNPS decommissioning, which have been carried out in the Nuclear Energy Agency of Organization for Economic Co-operation and Development (OECD/NEA), are introduced.

The knowledge quoted from the literature review and recent sim-debris tests were then compiled as a debris characteristic table by JAEA. Furthermore, core status maps and FP- and dose-distribution maps [6–8] were drawn for Unit 1, Unit 2 and Unit 3,

respectively, based on all relevant knowledge, including interior inspection, sample analysis and various sim-debris tests as well as severe accident analysis. The review of these maps was carried out under the IRID project by the experts’ group in which severe accident analysis and fuel/debris characterization experts of JAEA, TEPCO, the institute of Applied Energy (IAE), plant manufacturers and universities in Japan were gathered. These databases (debris characteristic table, core status maps, FP- and dose-distribution maps) were very important reference materials in the design studies of the FDNPS decommissioning.

2. Overview of investigation of the PCV inside

2-1. Objective and method for investigating of the PCV inside

In Unit 1, 2, and 3 of the FDNPS, degraded nuclear fuel is estimated to exist the inside of the RPV and PCV. This is so-called ‘fuel debris’ that once melted and re-solidified with a part of the reactor internals during severe accident progression. It should be retrieved and stored in a safe manner under stable conditions. Therefore, it is necessary to identify the conditions and characteristics of the fuel debris and where it exists. From 2015 to 2017, cosmic-ray muons that can pass through the reactor were used to investigate the major location of the fuel debris in each unit [9]. As a result of the muon tomography, the following outline information was obtained (this knowledge, although limited, was extremely beneficial in the very first stage):

Unit-1: high-density materials hardly existed in the reactor-core region;

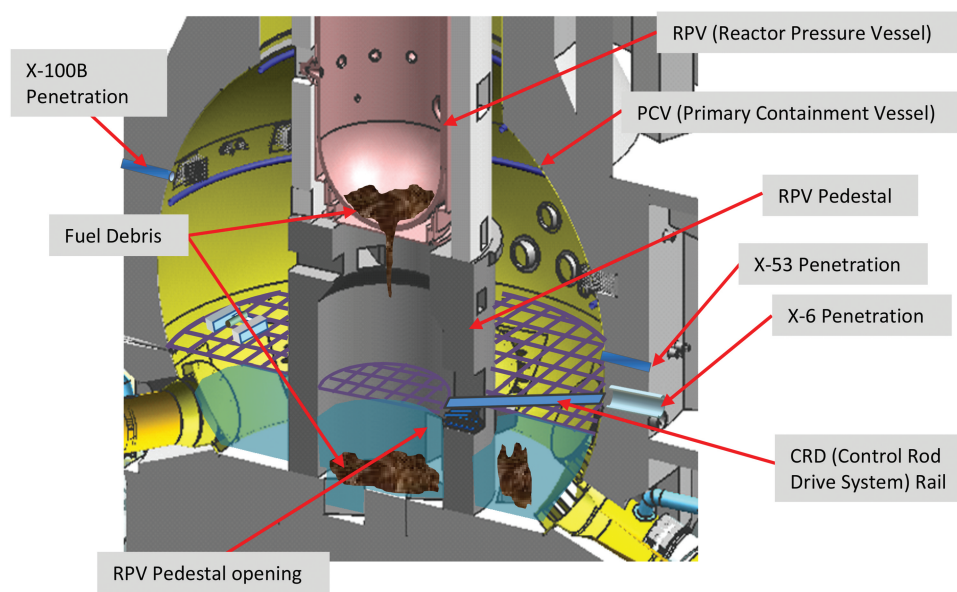


Figure 1. Schematic image of drywell (D/W) area of PCV (primary containment vessel).

Unit-2: high-density materials were detected to exist at the bottom of the RPV;

Unit-3: No large block of high-density materials was detected in the original reactor-core region, although a part of the fuel debris may exist at the bottom of the RPV.

Based on the obtained data of the high-density material distribution (assumed to be fuel debris), remotely operated technologies to explore the PCV inside of the three Units were developed, and on-site investigation was conducted for further details about the conditions of the fuel debris in each unit. It is of great importance to understand the detailed conditions (including the distribution of the fuel debris accumulations) to prepare for the fuel debris retrieval from the inside of the PCV.

2-2. Overview of investigation of the PCV inside in Unit 1

Figure 1 illustrates the inside of the drywell (D/W) of the PCV. The shape of the PCV looks similar to a flask. The RPV is located in the middle top center area of the PCV, which is supported by a cylindrical RPV pedestal made of reinforced concrete. The main body of the fuel debris is presumably located in the lower part of the RPV (in-vessel debris) and on the concrete floor inside/outside of the RPV pedestal (ex-vessel debris). The location of the X-100B and X-6 penetrations are also shown in the figure, via which the investigation robots enter into the PCV in Unit 1 and Unit 2 (see the following sections).

Muon inspection and severe accident analysis suggested that major parts of the fuel debris had likely spread out of the RPV and accumulated on the basement of the PCV of Unit 1 (i.e. the RPV pedestal and D/W areas of the PCV). Therefore, an on-site investigation was conducted for these areas by using a newly developed shape-changing crawler robot. In April 2015, the robot successfully accessed the inside of the PCV through the X-100B penetration, enabling the investigation of the 1st floor grating in the D/W of the PCV [10]. As a result of this investigation, the existing structures in the PCV were not significantly damaged. In parallel, radiation dose data were successfully obtained in three quarters of the 1st floor grating area.

In March 2017, the second trial of the D/W inside investigation was successfully carried out [11]. More detailed visual image data and radiation dose data were obtained using a small-size camera and a dosimeter attached to an improved shape-changing crawler robot that was hung from the 1st floor grating down to the bottom of the D/W of the

PCV. Figure S1 shows the appearance of the shape-changing crawler robot used for the second trial as indicated in [11].

The radiation dose around the X-6 penetration of Unit 1 was rather high. This is the penetration from which direct access to the inside of the RPV pedestal region had been originally planned. The extremely high dose does not permit workers to stay for long hours in the adjacent areas. Consequently, the X-6 penetration of Unit 1 has not been used as an access route for the robot yet.

The video images taken by the camera showed the accumulation of a sediment-like material at the bottom of the D/W of the PCV [12]. The accumulation of the sediment-like material on the top of the ex-vessel debris had not been originally expected from the accident progression analysis. Figure 2 indicates the appearance of the sediment material, which may reach several tens of centimeters in thickness on the original concrete floor or the ex-vessel fuel debris. A small sample was taken by the smear wipe of the robot, which was considered to contain a small amount of the sediment. The analysis was carried out in the hot cells of JAEA and Nippon Nuclear Fuel Development Co., Ltd. (NFD). The results indicated that major components are transition metals such as Fe, Cr, Ni, Mo and Zr and a small amount of U-bearing particles with a few micron size was contained in the sediment sample [13,14]. These data will be published in English journal shortly.

2-3. Overview of investigation of the PCV inside in Unit 2

Although a significant amount of the fuel debris is expected to accumulate in the lower part of the RPV, three investigations were conducted for the RPV pedestal area in the PCV for Unit 2. In Unit 2, a part of the fuel debris is considered to relocate from the RPV and accumulated in the pedestal area. Since the radiation dose around the X-6 penetration of Unit 2 was relatively lower than that in Unit 1, a robot was introduced via the X-6 penetration, which enabled direct access to the inside of the RPV pedestal. From January to February 2017, the investigation [15] was firstly conducted to explore the inside of the PCV by using a crawler-type remotely operated robot (Figure S2) [11]; however, it got stuck on materials accumulated on an inclined route (Control Rod Driving (CRD) rail) that connects the X-6 penetration and the pedestal entrance. Hence, unfortunately, the robot could not reach the inside of the RPV pedestal, since the probability of this kind of problem had already been discussed, an alternative plan was prepared, by which a pan-tilt camera attached on the head of a long pole entered the RPV pedestal through the X-6 penetration.

This alternative equipment successfully obtained visual images from the inside of the RPV pedestal. A large hole was observed in the grating of work platform, which was located off-center from the RPV pedestal center.

Later on, in January 2018, an improved investigation equipment that was mounted on a pan-tilt camera hung from a long pole head entered the RPV pedestal and provided more detailed images and dose data [16]. **Figure S3** shows the equipment used for the second access. The images showed a few pieces of a broken fuel assembly component (e.g. a part of top tie plate) were observed among the spreading materials on the RPV pedestal floor by the pedestal wall and the accumulation of pebble-like debris, including sediments, which was widely spread out on the concrete floor in the RPV pedestal area. The thickness of the pebble-like debris, which accumulates just beneath the previously observed hole, is larger than that of debris accumulating at other regions in the pedestal. One could conclude that a significant amount of molten corium had passed through the hole, which spread out from the off-center position of the RPV bottom head, as shown in [6–8]. Furthermore, it was observed that a small amount of deposits adhered to the CRD equipment. This could suggest a small failure at the RPV lower head and a leakage of the fuel debris.

In February 2019, the latest investigation was carried out using an investigation unit with movable tong-like fingers, which were installed on the head of the equipment beside the pan-tilt camera. The investigation unit was inserted into the RPV pedestal using the X-6 penetration. Then, the device hung on a wire was lowered down to investigate two areas, i.e. on the work platform and near the pedestal bottom. The finger directly contacted the sediments and solidified agglomerates and confirmed movable and non-movable materials on the metallic wall of a cable tray in the pedestal bottom and on the grating of the work platform, respectively (**Figure 3**) [17,18]. The operation confirmed that the movable finger is able to grip, lift and move small size debris approximately 5–75 mm in size as estimated by Pshenichnikov et al. [19].

Careful observation of the visual images indicated that the accumulates were roughly divided into three types, (i) once molten metal-rich debris, (ii) degraded (once molten) oxidic debris, and (iii) once partially melted and mechanically slumped core materials (e.g. a part of top tie plate) [20–23]. Furthermore, the similarity was noted between these visual images of PCV accumulates and the appearance of metal-rich sim-debris in the integral tests for the control blade degradation at JAEA/CLADS as discussed in [20–23].

These observations and investigations resulted in understanding that two debris relocation paths seem possible for Unit 2: (i) minor breaches near CRD joints with the gradual melt release in small amounts

and likely in several places simultaneously and (ii) one major breach with a release of a large amount of molten corium with a small amount of the non-melting core components. The latter relocation could happen in a short time, which could enable the redistribution of heat source from the lower plenum of RPV to the pedestal region and result in a decrease in debris temperature.

No significant interaction was observed between the solidified stone-like debris and steel materials such as a cable tray in the pedestal bottom. This might be a sign of the initially low thermal energy of the relocating debris and the absence of the significant temperature re-increase due to decay heat or chemical interactions in the pedestal region. Furthermore, **Figure 3(b)** shows that a part of relocating debris was stuck on the grating and the appearance seemed to be a solidified alloy. These investigations could indirectly imply that the relocating debris was mostly metallic and also these might be a sign that the major heat source (the oxidic debris) helped the preceding liquefaction of the metal-rich debris in the lower plenum of the RPV.

2-4. Overview of investigation of the PCV inside in Unit 3

The water level in the PCV of Unit 3 is higher than that in Unit 1 and Unit 2, which means that almost all fuel debris accumulated in the RPV pedestal is covered with water. For this reason, an underwater remotely operated vehicle (ROV) [11] was developed (**Figure S4**) to investigate the inside of the PCV in Unit 3, including the RPV pedestal area. The underwater ROV entered the PCV through the X-53 penetration because the X-6 penetration in Unit 3 was submerged. This investigation was conducted in July 2017 [16].

TEPCO made a 3D-image of the inside of the RPV pedestal using visual data recorded by the underwater ROV, as illustrated in **Figure 4** [24]. A significant amount of the fuel debris accumulated in the RPV pedestal. The thickness reached approximately 3 m in maximum from the original concrete floor level. The apparent volume of the accumulated materials was a few times larger than the volume of the original core materials calculated from theoretical densities. This could suggest that the fuel debris is likely to be porous or to have many internal vacancies or holes. Several segments of severely damaged internal steel materials were observed to penetrate into the fuel debris body. In addition, a small mountain-like accumulation was observed in the center top region of the fuel debris. These observations could suggest that the fuel debris is likely to a mixture of solid and liquid during the relocation from the RPV and hence the temperature during the relocation might be rather lower than the liquefaction temperature of the oxidic fuel debris. According to the phase diagram between UO_2 and ZrO_2 [25], the

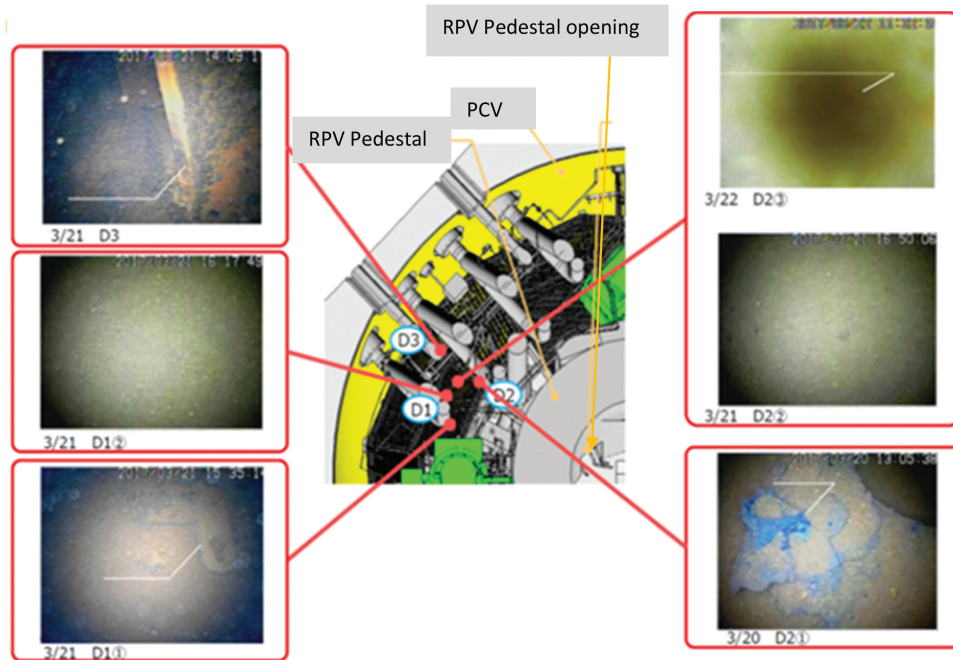


Figure 2. Appearance of sediment materials accumulated in the D/W bottom of Unit 1 [12].



Figure 3. Investigation for the sediments (a) accumulated on the cable channel [17] and (b) adhered to the grating in the RPV pedestal [18].

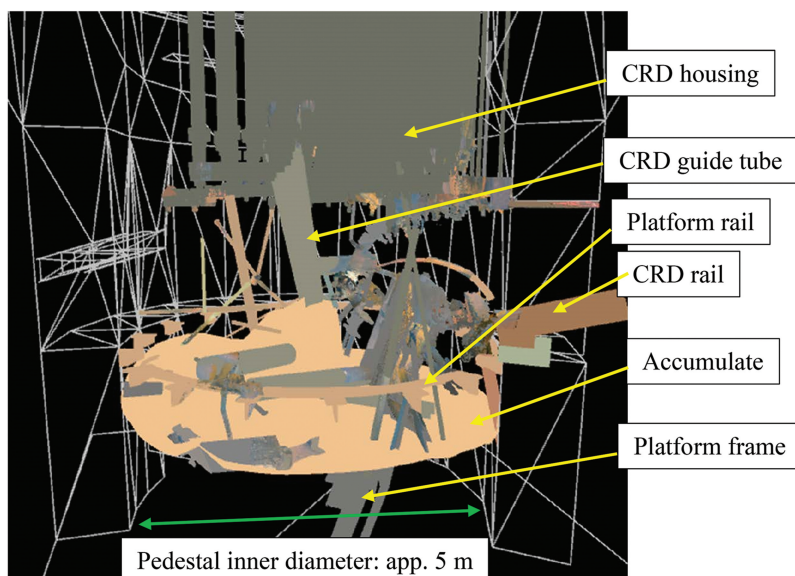


Figure 4. 3D image of the inside of Unit 3 RPV pedestal [24].

temperature to form fully molten oxidic fuel debris during the in-vessel accident is at approximately 2550 °C or a little higher. Therefore, in Unit 3, the relocation of partially-molten oxidic debris was probably at a few hundred degrees below 2550 °C. These investigations could also predict that the relocation of such a large volume of fuel debris (mixed with solid and liquid) needed a certain time (presumably a few hours). Regarding the RPV lower head and the original adjacent structures, the video image showed the severe damage of these materials. A part of CRD and the support materials had relocated into the fuel debris. These facts are also consistent with the inference that the debris temperature did not reach the value for full liquefaction and that the partially-molten corium was gradually relocated to the pedestal region.

2-5. Planning investigations of the PCV inside (current status as of March 2021)

As stated in the above sections, the conditions of the inside of the PCV have become gradually clear. New equipment is being developed to acquire more information for further use.

A new boat-type submarine has been developed to access and investigate the inside of the PCV in Unit 1 (Figure S5) [11]. This equipment has a total length of approximately 1100 mm, a cylindrical shape with a diameter of 250 mm, and various sensors: a scanning-type ultrasonic distance meter to acquire data on the shape of the sediments accumulated on the bottom of the PCV, a high-power ultrasonic sensor to measure the thickness of the sediments, a radiation-measuring instrument to qualify the distribution of fuel debris, etc. Each measuring device to be installed is specialized for the boat-type access equipment. A further boat-type access piece of equipment was prepared to obtain small sediment samples. Smaller equipment is also planned for investigating the inside of the RPV pedestal using the pan-tilt camera. IRID is also developing the technology for building an access route that can safely insert

this equipment to investigate a wider range of location for a longer time, as well as various sensors with improved resistance to radiation.

Concerning Unit 2, a detailed investigation will be carried out to access the PCV inside through the existing X-6 penetration route. Furthermore, an arm-type access device (Figure S6) is being developed for small retrievals of the fuel debris from the pedestal region [26]. This equipment features a total length of approximately 22 m. The arm can be folded for storage in a box (enclosure) connected with the exterior of the PCV before use, and sequentially unfolded to enter the PCV at the time of use. The arm head is capable of accepting other equipment up to approximately 10 kg. Figure 5 shows an illustration from the investigation of the inside of the PCV using arm-type access equipment [26]. The investigation is planned such that the arm stored in the enclosure will pass through the PCV connecting structure and then access the PCV through the X-6 penetration as shown in [26].

2-6. Expectation for sampling analysis, fuel debris characterization, and identification of the inside of the reactor

The retrieval of the fuel debris is planned to gradually start in the near future. It is essential to identify the debris properties and then to improve them with experience. Identifying the composition of the fuel debris and its mechanical, chemical and radioactive properties is necessary to retrieve and sort the fuel debris after retrieval. Various studies have been previously conducted based on the relevant knowledge of the TMI-2 accident. The FDNPS accident is an unprecedented disaster and had special circumstances in which nuclear fuel melted and penetrated the RPV bottom, and a part of molten core materials (corium) might be solidified with molten concrete at the bottom of the PCV. These processes in accident sequence (ex-vessel phases) go further than those observed in TMI-2 (only in-vessel phase) and in particular require a detailed knowledge of the ex-

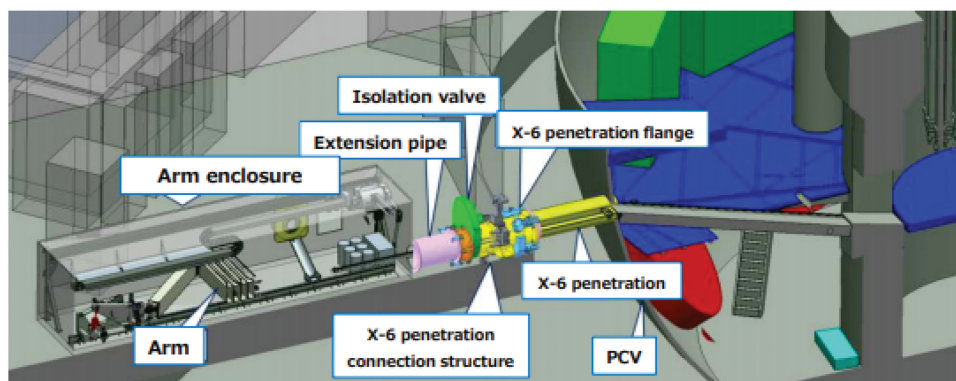


Figure 5. Installation of arm-type access equipment [26].

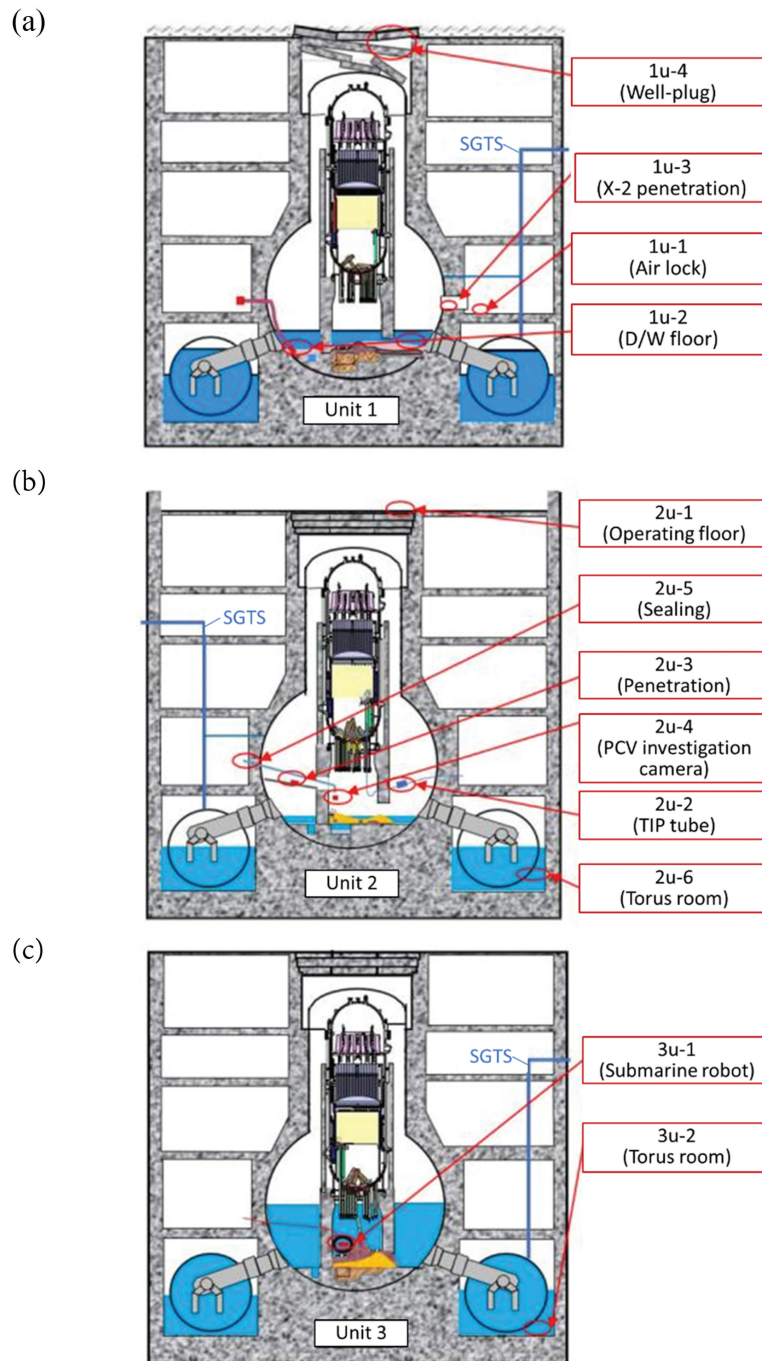


Figure 6. Sampling position of the FDNPS samples [27]. (a) Unit 1, (b) Unit 2, (c) Unit 3.

Table 1. Sampling position and sample ID.

Unit number	Position	Sample ID number (used in the present review)
Unit 1	The air-lock of the R/B	1 u-1
	The sediment accumulated in D/W	1 u-2
	the blockage material accumulated in the X-2 penetration	1 u-3
	the well plug in the operation floor	1 u-4
Unit 2	the deposit on a blue sheet covering on the well plug in the operation floor	2 u-1
	the deposit in the TIP tube	2 u-2
	the blockage material accumulated in the penetration	2 u-3
	the smear paper of the investigation video camera	2 u-4
	the smear paper of the investigation video camera (2 u-4) and the sealing	2 u-5
	the filtered sample of stagnant water collected in the torus area	2 u-6
Unit 3	the smear paper of the submarine robot	3 u-1
	the filtered sample of stagnant water collected in the torus area	3 u-2

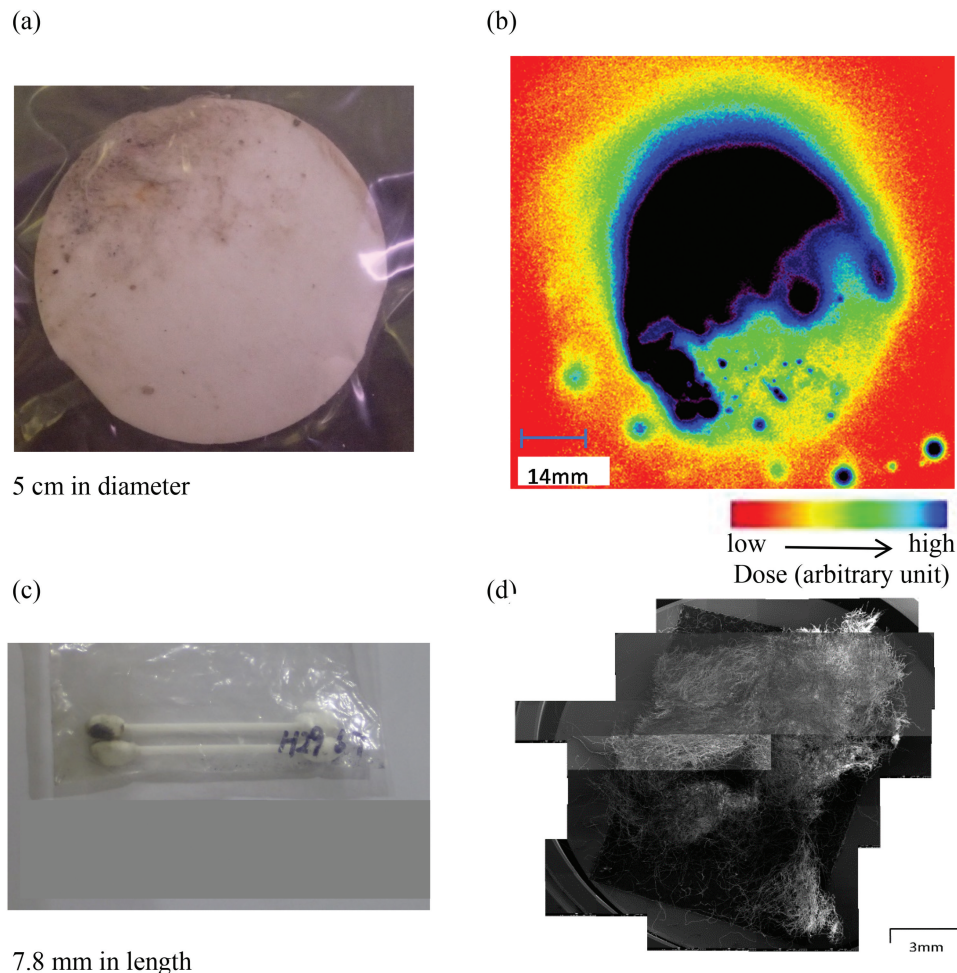


Figure 7. (a) Appearance of 1 u-4 smear sample and (b) the IP analysis data (c) Appearance of 2 u-3 cotton swab sample and (d) the SEM image data (low magnification) [27].

vessel fuel debris characteristics. The fuel debris sampled from a small retrieval at the first stage will be analyzed comprehensively, and then the properties of the ex-vessel fuel debris will be identified. Exhaustive studies on the fuel debris will still be necessary. In the future, it will be a significant issue to understand the conditions (as yet uncertain) of the inside of the RPV to be able to retrieve fuel debris from the RPV in the optimum way.

3. Current status of the samples taken from the inside of the PCV and R/B

3-1. Outline of sampling position and appearance

Figure 6 indicates the areas from which a small amount of samples were taken during the investigation of the PCV and R/B insides [27]. Table 1 shows the details of these samples and the ID number for analysis. Each sample contained a few pieces of smear paper, cotton swab, and plastic bottle and the weight is approximately several tens of mg to several hundreds of mg. In the present review, the simplified ID numbers, such as

1 u-1 ~ 1 u-4, 2 u-1 ~ 2 u-6, and 3 u-1 ~ 3 u-2, are used for convenience. Four samples were taken from Unit 1, such as the white-colored powder accumulated in the air-lock of the R/B (1 u-1), the sediment accumulated in D/W (1 u-2), the blockage material accumulated in the X-2 penetration (1 u-3) and the smear paper of the well plug in the operation floor (1 u-4). Six samples were taken from Unit 2, such as the deposit on a blue sheet covering on the well plug in the operation floor (2 u-1), the deposit in the TIP tube (2 u-2), the blockage material accumulated in the penetration (2 u-3), the smear paper of the investigation video camera (2 u-4) and the sealing (2 u-5), and the filtered sample of stagnant water collected in the torus area (2 u-6). Then, two samples were taken from Unit 3, such as the smear paper of the submarine robot (3 u-1) and the filtered sample of stagnant water collected in the torus area (3 u-1).

Figure 7 shows a few examples of the samples' appearance. Imaging plate (IP) analysis showed the contamination of the smear papers and low magnification SEM analysis showed the accumulation of powder- or particle-like materials on the smear paper or cotton swab [27].

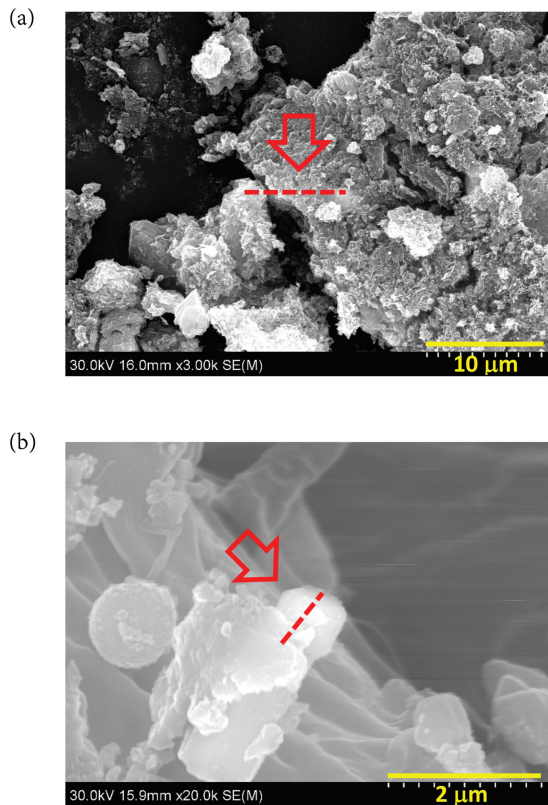


Figure 8. SEM image of typical U-bearing particles (a) taken from 1 u-2 (the PCV inside) and (b) taken from 1 u-4 (the PCV outside) [27]. The dashed lines and the block arrows indicate the cross section and the direction of observation for TEM analyses in Figure 9, respectively.

3-2. Analysis method

The following analysis flow was in general used for these samples. After getting the appearance image and the dose data, the IP analysis was carried out for each sample paper. Regarding the cotton swab and filtered sediment samples, these deposited materials were once adhered to a smear paper and then analyzed by IP. Then, the contaminated areas were identified from the IP images. A few pieces were cut from the contaminated areas and were analyzed by SEM/EDX, SEM/WDX and TEM analysis, whereas the others were analyzed by ICP-MS and radiation analysis after dissolving them in nitric acid with a small amount of hydrofluoric acid or aqua regia. The oxidation status of uranium 'so-called O/U ratio' is one of the most important data to characterize debris samples. However, it is rather difficult to measure precisely the oxygen concentration in these FDNPS samples by currently available analysis techniques.

3-3. Outline of Unit 1 sample analysis

The detailed data of the sample analysis will be published shortly [28] and the present review attempts to outline the knowledge obtained from the analysis.

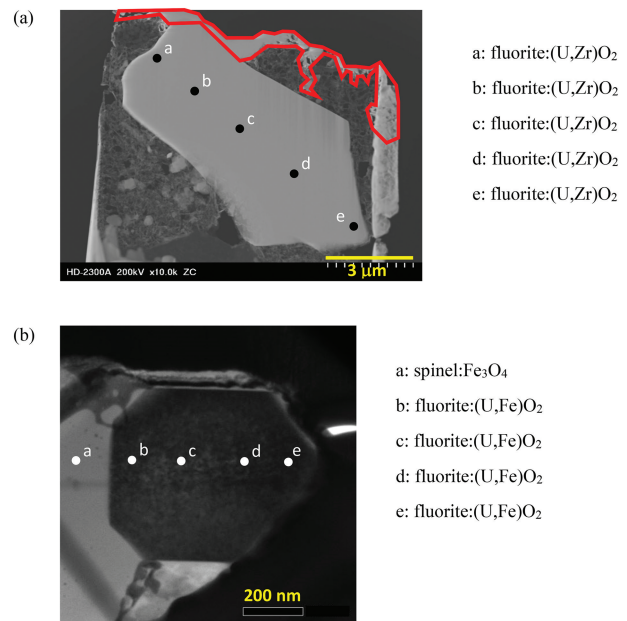


Figure 9. TEM image of typical U-bearing particles and phases detected from the EDX point analyses: (a) taken from 1 u-2 (the PCV inside) and (b) taken from 1 u-4 (the PCV outside) [27]. Solid circles indicate the EDX analysis point. The red colored region corresponds to W-protection. (a) a: fluorite:(U,Zr)O₂. b: fluorite:(U,Zr)O₂. c: fluorite:(U,Zr)O₂. d: fluorite:(U,Zr)O₂. e: fluorite:(U,Zr)O₂. (b) a: spinel:Fe₃O₄. b: fluorite:(U,Fe)O₂. c: fluorite:(U,Fe)O₂. d: fluorite:(U,Fe)O₂. e: fluorite:(U,Fe)O₂.

Regarding actinide elements, U and Pu were detected in all samples. In 1 u-2, 1 u-3 and 1 u-4, U and Pu were mainly contained in particles of a few to approximately 10 microns in size (hereafter, named as U-bearing particles), whereas in 1 u-1 only a trace amount of U and Pu were detected by the ICP-MS analysis. Furthermore, a trace amount of Am was detected in 1 u-1 and 1 u-2 and of Cm in 1 u-2, respectively. Figure 8(a) and Figure 8(b) show the SEM image of the typical U-bearing particle contained in 1 u-2 (the PCV inside) and 1 u-4 (the PCV outside) samples, respectively [27]. In all U-bearing particles analyzed, Pu was detected almost overlapping the region where U was detected. Although the number of U-bearing particles already analyzed was limited, the Pu/U molar ratio in 1 u-3 and 1 u-4 (the PCV outside) was a few times larger than that in 1 u-2 (the PCV inside). We need detailed analysis to quantify the tendency. A small amount of Zr also contained in these U-bearing particles. According to the EDX point analysis and the ZAF correction of the U-bearing particles, the Zr/U molar ratio was almost fixed to be 5/95, 10/90 and 2/98 in the 1 u-2, 1 u-3 and 1 u-4 samples, respectively, with several exceptions. The EDX point analysis also detected Fe, Ni, Cr, Mo, Zn, Si and Al in or around the U-bearing particles. Considering the particle size, the detected EDX values may be influenced by the materials which surrounded

the particles. One needs to take into consideration that these EDX analysis results by TEM or SEM do not show the composition of U-bearing particles themselves but shows the average composition of U-bearing particles + surrounding area. Although the sample number was limited, the molar ratios of Mo, Zn, Na and Al to U in the U-bearing particles in 1 u-2 (inside of the PCV of Unit 1) were a few times larger than those detected in the PCV inside samples for Unit 2 and Unit 3. We need the further analysis for fuel debris samples to confirm the significance of these tendencies in the near future.

The TEM analysis was carried out for small thin samples taken from the several U-bearing particles. Figure 9(a) and Figure 9(b) indicate the TEM image and the phases detected at each analysis point for the U-bearing particles taken from the 1 u-2 and 1 u-4 samples, respectively [27]. The difference in phase structure is still being discussed in these samples. Currently fluorite phase with a face-centered cubic (fcc) structure (hereafter, named as fluorite) was detected as a dominant phase in 1 u-2, in which U and Zr coexisted with almost fixed molar ratios with a small amount of Fe and Cr. Since the dominant components are U and Zr, the fluorite phase is shown as (U,Zr)O₂ in the figure. On the other hand, a fluorite phase with a different composition were detected in 1 u-4, in which the major components are U and Fe (with a very limited Zr). A small amount of monoclinic Zr-rich phase was also detected, but considering the current uncertainty of EDX, the result is still under discussion. These differences in phase composition may be caused by the difference in formation mechanism of these particles. According to Mizokami et al. [29], two prototypic formation mechanisms could be inferred as Type-I and Type-II. The Type-I particle is expected to be formed by the solidification from a molten material, whereas the Type-II by the condensation from a gas phase. Due to the low volatility of Zr-oxide, Zr is considered to be hardly transported via a gas phase. Based on these phase composition and chemical status data for the U-bearing particles, it is expected the chemical condition of the fuel debris during the accident progress can be estimated. The detailed analysis is still ongoing.

The ICP-MS and radiation analysis detected many nuclides contained in the samples, which are roughly categorized to be actinides (U, Pu, Am, Cm), cladding or channel box (Zr), steel (Fe, Cr, Ni, Co, Mn, Sn, Ti, Cu, Mo), paint or shielding (Zn, Al, Pb), fission products (Sr, Rb, Y, Sb, Te, Cs, Ba, RE; RE = rare earth elements), light elements (B, Si, Na, Mg, Al, Ca) and others (Bi, W). The origin of Al, Si and Ca may well be concrete materials but there are other possibilities (e.g. insulator) and this matter is still under discussion. The isotopic ratio between ²³⁵U and ²³⁸U for Unit 1 samples is mostly comparable to that of the average value of the original core (²³⁵U/²³⁸U = 0.017) [30]. This suggested

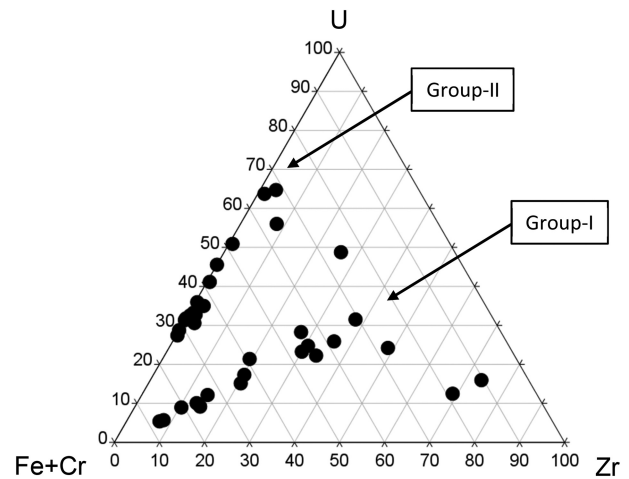


Figure 10. Composition triangle among mole amounts of U, Zr and Fe+Cr detected by the EDX point analysis for U-bearing particles (influenced by surrounding materials) in 2 u-1 sample which was taken from the operation floor [27].

that the origin of U detected in these samples is the unit's nuclear fuel. Trace amounts of Mo were detected in all Unit 1 samples. The isotopic ratio among ⁹⁵Mo, ⁹⁷Mo, ⁹⁸Mo and ¹⁰⁰Mo is reasonably comparable to the natural isotopic ratio (approximately 27:16:41:16, when normalizing by sum of the above-mentioned four isotopes) with the exception of 1 u-2. This suggested the origin of Mo detected in 1 u-1, 1 u-3 and 1 u-4 samples is presumably Mo-grease for the steel materials. As for the 1 u-2 sample, it was difficult to evaluate the isotopic ratio due to the very low Mo-contents. According to TEPCO, certain amounts of Zn, Al and Pb were originally contained in the paint of PCV wall, thermal shield and radiation shield. The origin of B is presumably a neutron absorber material. These analysis results indicated that these elements detected in the above samples could be also contained in the ex-vessel fuel debris.

3-4. Outline of Unit 2 samples

Regarding 2 u-1 (which was taken from the operation floor), various volatile and non-volatile elements were detected. As for the proper discussion on volatility, one needs to define volatile and non-volatile elements at accidental conditions. The volatile and non-volatile elements were previously categorized by Grambow et al. [31], in which (i) fission gases (Xe, Kr), I, Cs, Rb, Sb, Te, Cd, and Ag are categorized as volatile, (ii) Ba, Mo, Tc, Ru, and Pd as semi-volatile, (iii) Sr, Nb, Rh, Y, La, Ce, and Eu as low-volatile, and (iv) Zr, Nd, Pr, and actinides (U, Np, Pu, Am, Cm) as non-volatile. This clarification is used in the present review. Also, lots of U-bearing particles were detected in the 2 u-1 sample. We attempted to draw a composition triangle among the mole amount of U, Zr and Fe+Cr determined from the EDX point analysis for the U-bearing particles, as shown in Figure 10 [27]. Although the molar ratios between U and Fe+Cr and between Zr

and Fe+Cr are widely scattered (due to the influence of surrounding area), the molar ratio between U and Zr is clearly categorized into two groups with a few exceptions. We categorized these two groups as Group-I and Group-II in the present review. In the Group-I particles, the Zr/U molar ratio is around 1/1 and TEM analysis suggested that Zr and U homogeneously coexisted in the fluorite phase. On the other hand, in the Group-II particles, Zr was hardly detected and U and Fe homogeneously coexisted in the fluorite phase (but, the Fe-amount is rather influenced by surrounding materials). A small region with the spinel phase was also detected in the Group-I particles. These results suggested that the Group-I particles are likely to form via a quick solidification from the molten material (Type-I mechanism, as described above) and the Group-II particles via a condensation from the gas phase (Type-II mechanism, as described above). These results suggested that at least two mechanisms could be considered for the transportation of the U-bearing particle. Furthermore, the ICP-MS analysis of the 2 u-1 sample identified both volatile and non-volatile elements. The origin of Mo is presumably from FP (which was evaluated from the isotopic ratio). The Ni/Fe and Cr/Fe ratios are relatively smaller than those of other Unit 2 samples.

Regarding samples taken from the inside of the PCV (2 u-2 ~ 2 u-5), the analysis results are slightly different from each other. As for 2 u-2 (deposit in TIP tube), the ICP-MS analysis detected similar nuclides with those detected in 2 u-1 (operating floor). However, due to the very small values for U-isotopes for 2 u-2, the origin of U is still under discussion. Currently, no U-bearing particles were detected by the SEM/EDX and SEM/WDX analysis for 2 u-2 although U, Pu and Am were detected by the ICP-

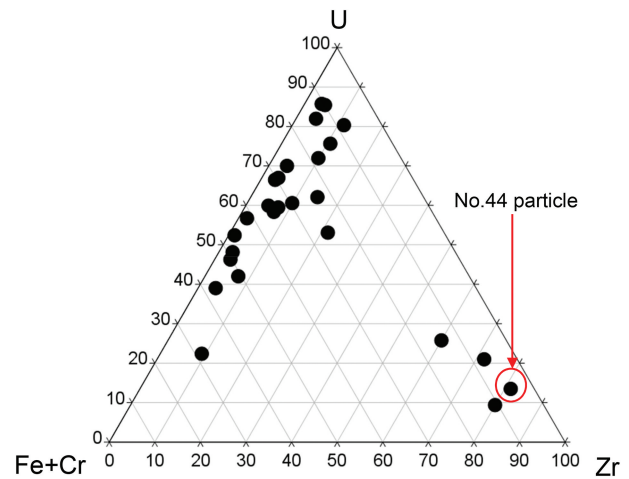
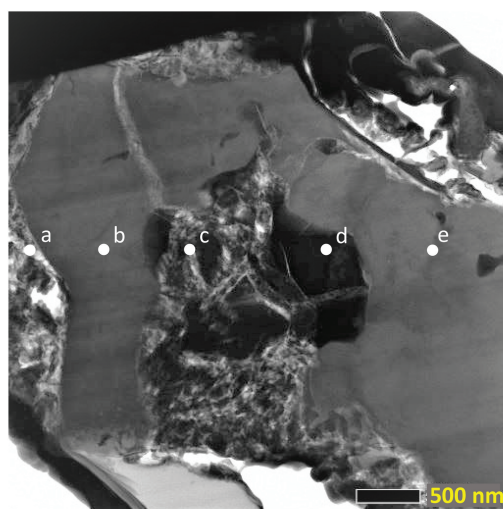


Figure 11. Composition triangle among mole amounts of U, Zr and Fe+Cr detected by the EDX point analysis for U-bearing particles (influenced by surrounding materials) in 3 u-1 sample [27].

MS analysis. The EDX area analysis showed that close association between Cr and Mn, between Fe and Ni, and among Si, Al and Na, whereas the clear separation between Fe and Zr. The isotopic ratio of Mo could infer the origin was Mo-grease (natural isotopic ratio). These analysis results could also suggest the existence of metal-rich debris.

In the 2 u-3 sample (blockage material in the X6 penetration), both volatile and non-volatile materials were detected by the ICP-MS analysis. Only a few U-bearing particles were detected by the SEM/WDX analysis (not analyzed by TEM yet).

As for the 2 u-4 sample (smear of video camera), only the microscopic analysis was carried out, which detected several U-bearing particles. Pu homogeneously coexisted with U in the particles. The U/Zr molar ratio in the U-bearing particles in 2 u-4 was



- a: fluorite:(U,Fe,(Zr))O₂ + spinel:(Fe,Cr)₃O₄
- b: tetragonal:(Zr,(U))O₂
- c: fluorite:(U,Fe,(Zr))O₂ + spinel:Fe₃O₄
- d: fluorite:(U,Fe,(Zr))O₂ + spinel:(Fe,Cr)₃O₄
- e: tetragonal:(Zr,(U))O₂

Figure 12. Example of TEM image and phases detected in U-bearing particle in 3 u-1 (no. 44 particle) [27]. a: fluorite:(U,Fe,(Zr))O₂ + spinel:(Fe,Cr)₃O₄. b: tetragonal:(Zr,(U))O₂. c: fluorite:(U,Fe,(Zr))O₂ + spinel:Fe₃O₄. d: fluorite:(U,Fe,(Zr))O₂ + spinel:(Fe,Cr)₃O₄. e: tetragonal:(Zr,(U))O₂

largely scattered and this is the unique feature of this particular sample. The TEM analysis identified only a fluorite phase for the U-bearing particles. These could suggest that these U-bearing particles formed via a quick cooling or a direct fragmentation of molten oxidic corium.

As for the 2 u-5 sample (smear of sealing), only the ICP-MS analysis was carried out. Both volatile and non-volatile materials were detected in 2 u-5. The isotopic ratio between ^{235}U and ^{238}U inferred the origin of U was fuel. However, further analysis is necessary to confirm this prediction.

3-5. Outline of Unit 3 samples

Only 3 u-1 sample was currently collected from the inside of the PCV of Unit 3. Nuclides or materials detected in 3 u-1 were mostly similar to those detected at the inside of the PCV samples for Unit 1 and Unit 2. The only clear difference for the ICP-MS analysis results for 3 u-1 is the relatively smaller amount of Pb and Zn than other units' samples. The isotopic ratio for $^{235}\text{U}/^{238}\text{U}$ pointed to a likely origin of nuclear fuel. The SEM/EDX and SEM/WDX analysis detected several tens of U-bearing particles with different features from those detected in Unit 1 and Unit 2 samples. Figure 11 indicates the composition triangle of the U-bearing particles detected in 3 u-1, which were obtained from the EDX point analysis and the ZAF correction (hence, probably influenced by the surrounding materials) [27]. Lots of the particles have small values for the Zr/U molar ratio, which is roughly varied between approximately 2 and 12 mol%Zr. However, we also detected several particles having clearly higher Zr/U molar ratio. The TEM analysis identified four phases in the U-bearing particles with the different phase fractions depending on the particles,

such as fluorite:(U,Fe,(Zr))O₂, tetragonal:(Zr,(U))O₂, α -Zr(O) and spinel:(Fe,Cr)₃O₄. Here, the brackets mean that the corresponding element was detected as a very minor component in respective phases. The fluorite:(U,Fe,(Zr))O₂ and spinel:(Fe,Cr)₃O₄ phases detected by TEM probably correspond to the U-rich particles detected by SEM/EDX; the larger analyzed zones of EDX (~1 μm) would be expected to give combined particle analyses compared to the typical ~50 nm analysis zone of TEM. The Zr-concentration in the U-rich fluorite phase is rather limited, whereas the U-concentration in the Zr-rich tetragonal phase is limited. Furthermore, the microstructure of the U-bearing particles detected in the 3 u-1 sample had unique complicated features which were not found in the Unit 1 and Unit 2 samples until now. Figure 12 indicates this complex phase structure of the U-bearing particles in 3 u-1 [27]. Two regions are clearly observed even in this very small sample, such as porous regions observed in the middle and left and plane dense regions in the periphery, respectively. The major phases identified for the porous region were fluorite:(U,Fe,(Zr))O₂ and spinel:(Fe,Cr)₃O₄, and whereas only tetragonal:(Zr,U)O₂ were identified in the dense (polished) region. This unique feature indicated multiple formation mechanisms for the U-bearing particles detected in Unit 3. The details are discussed elsewhere currently only in Japanese [27,32] and published in English shortly within 2022 [28].

3-6 Outline of samples taken from torus room

In this section, the features of 2 u-6 and 3 u-2 samples are outlined, which were collected from the retained water in each torus room, respectively, as shown in Figure 12 [27]. The ICP-MS analysis could identify a few unique features for these torus room samples

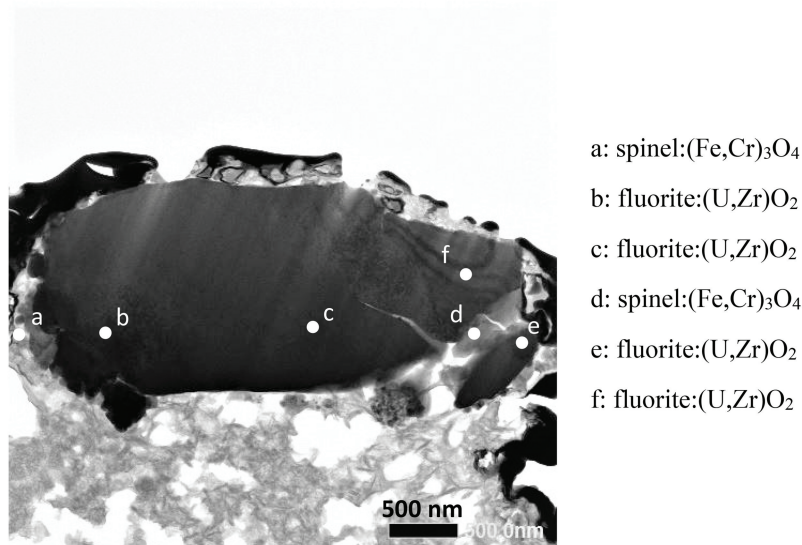


Figure 13. Example of TEM image and phases detected in U-bearing particle in 2 u-6 (no. 1 particle) [27]. a: spinel:(Fe,Cr)₃O₄. b: fluorite:(U,Zr)O₂. c: fluorite:(U,Zr)O₂. d: spinel:(Fe,Cr)₃O₄. e: fluorite:(U,Zr)O₂. f: fluorite:(U,Zr)O₂

compared to the samples taken from the inside of the PCV: Mo was not detected, Ce only detected among RE-elements and Ni/Fe and Cr/Fe ratios were lower. Several U-bearing particles were detected in these torus room samples. The SEM/WDX analysis shows a few times larger Pu/U molar ratio in 2 u-6 than those samples from the inside of the PCV (not yet determined for the 3 u-2 sample). Figure 13 indicates some of the TEM analysis for 2 u-6 [27]. The TEM analysis mostly identified the fluorite and spinel phases in the U-bearing particles. The fluorite phase contained mainly U, Zr, Fe and Cr. The homogeneous distribution in the composition of the fluorite phase could infer a Type-I formation mechanism for these particles. In addition, a small amount of Cr_2O_3 was detected in 2 u-6. This could imply the presence of uranium in higher oxidation state (U^{+5}) or slightly hyper-stoichiometric phase (UO_{2+x}). In fact, a UO_2 particle was detected in SEM/EDX and TEM analysis for 2 u-6. The origin was still under discussion (possibly, a fragment of UO_2 pellet or a Type-II particle). These results would hint at the further oxidation of the U-bearing particles during the transportation via coolant water.

4. Preliminary studies for debris characterization using surrogate materials and debris analysis

Understanding for the fuel debris characteristics (mechanical, chemical, thermal and radioactive properties as well as microscopic or macroscopic appearance or agglomeration) and accident progression scenario of in-vessel conditions was mainly based on the TMI-2 accident (as a prototypical PWR accident). Since the FDNPS accident happened in BWR and the significant amount of fuel debris was relocated to ex-vessel, we are faced with several important knowledge

gaps just after the FDNPS accident. JAEA took the initiative in R&Ds on foreseen issues in the FDNPS decommissioning immediately after the accident, and led the fuel debris characterization projects [32]. Extensive R&Ds have been performed, as reported in [32,33]. This chapter outlines main insights obtained from those R&Ds.

4-1 Prioritization of R&D issues for characterizing fuel debris generated at the FDNPS

The most important requirement for the fuel debris characterization immediately after the FDNPS accident was to summarize comprehensively the previous knowledge on designing processes and tools regarding fuel debris retrieval and then to identify the knowledge gap for the fuel debris retrieval at the FDNPS [33]. First, the debris retrieval experiences at TMI-2 were investigated, and tools or equipment utilized in the TMI-2 decommissioning were categorized, as shown in Figure 14 [33,34]. The tools and equipment were roughly classified into six types according to assumed debris forms. Then, the JAEA preliminarily categorized the fundamental chemical, mechanical and thermal properties of fuel debris by literature survey, thermodynamic evaluation and small-scale tests. These properties were organized in terms of various requirements of debris retrieval (the report [33,34] was used as the first step knowledge base). Several important concerns were identified in these preliminary studies and the following information exchange with equipment designers [33,34]. As for designing retrieval tools, we needed to further accumulate mechanical properties including hardness, fracture toughness, and elastic modulus firstly and then we have been gathering the data for other important characteristics (e.g. porosity, fissile concentration). When thermal cutting methods are being applied, more reliable melting temperature

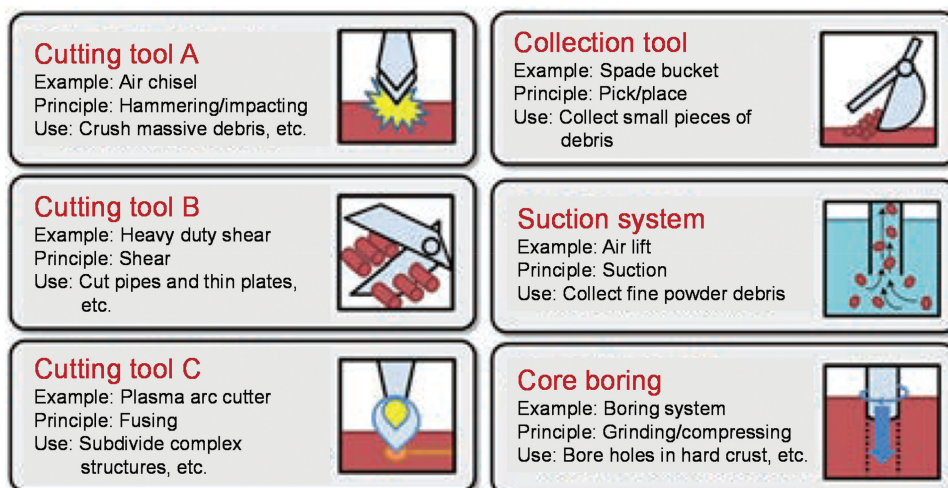


Figure 14. Classification of retrieval tools utilized in TMI-2 decommissioning [33,34].

data of various types of fuel debris at the FDNPS will be necessary. The results of characterization are described in the following sections 4-2 to 4-4.

In addition, two important concerns have been pointed out during the continuous information exchange for designing fuel debris retrieval in the late 2010s. The first issue is leaching of radionuclides from the fuel debris into adhering water. A few decades will be necessary for the completion of the debris retrieval for each unit. The influence of longer-term dissolution/transportation/deposition of FP and surface degradation of fuel debris body requires evaluation and this needs investigation of the relevant fundamental knowledge. The second issue is dust/aerosol formation/transportation during the retrieval processing. It is of great importance to study the size distribution in the dust/aerosol formed in cutting processes, and its transportation/deposition behaviour. These additional concerns are highly relevant to radiation protection of workers involved in the decommissioning operation. The current results of these two issues are discussed in section 4-5.

Establishing debris analysis technology is another important challenge for decommissioning. No core drilling is currently planned for debris sampling at the FDNPS site, which was applied for TMI-2 investigation and showed useful knowledge on the damaged status of the RPV inside. Instead, a gradual increase in recovery amount from a few g-scale is being considered. Then, at the stage when the fuel debris will be recovered continuously, a typical sample size for analysis is expected to be on the kg-scale in a single campaign. Concerns regarding the analysis of several kg-scale of 'poorly characterized' FDNPS fuel debris analysis are discussed in section 4-6.

4-2 Thermodynamic evaluation of the FDNPS debris

To obtain the preliminary insight of the fuel debris chemical characteristics, thermodynamic equilibrium calculation and various sim-tests have been carried out to predict prototypic phase/element compositions of in-vessel and ex-vessel debris generated in the FDNPS accident conditions. In the thermodynamic evaluation, FactSage ver 6.2 [35] and NUCLEA [36] were used for the calculation tool and thermodynamic database, respectively. This evaluation used the amount of original core materials and performed the sensitivity analysis by varying temperature, composition and oxidation progress, which was able to infer the probable range in the phase/element composition of in-vessel debris [37,38]. By referring to the analysis results using MELCOR 1.8.5 [39], the localization of the debris phase composition in the RPV was investigated. These calculation results suggested that fluorite (U,Zr)O₂ phase is likely to be dominant in the oxidic debris of the FDNPS as in the TMI-2 investigation. Furthermore, if U-metal was formed during accident progress, Fe₂(Zr, U) could be a major metallic phase as discussed in [37]. As for the ex-vessel debris, Kitagaki et al. [38] showed in their thermodynamic evaluation that almost all U and Zr could be contained in (U,Zr)O₂ and (Zr,U)SiO₄ phases. These preliminary calculation results were useful for identifying the knowledge gap and conducting small-scale tests for the FDNPS debris characterization. For example, the influence of core materials for BWR (a significant amount of B₄C absorber and far larger amounts of zircaloy (Zry) and stainless steel (SS) than prototypic PWR) and those of seawater components needed to be further studied.

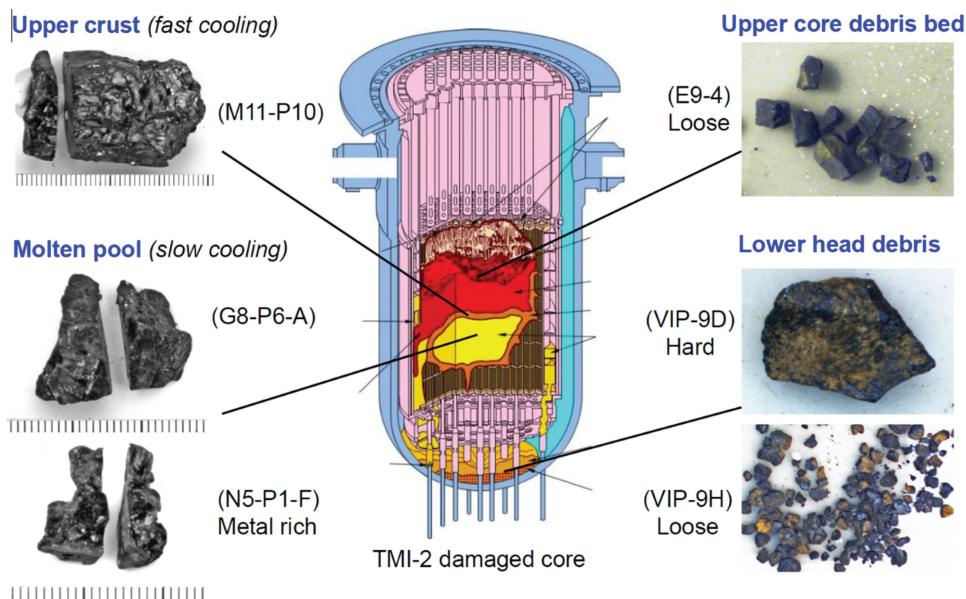


Figure 15. TMI-2 debris samples used for re-characterization analyses [44].

4-3 Debris characterization using surrogate materials

As mentioned above, the improvement of mechanical properties of the (U,Zr)O₂ base oxide was necessary, which could be a main component of both in in-vessel and ex-vessel fuel debris at the FDNPS. Hoshino et al. [40] and Kitagaki et al. [41] acquired Vickers hardness, elastic modulus, and fracture toughness of sintered U_{1-x}Zr_xO₂ pellets with varying Zr contents (x-value). They revealed that Vickers hardness was drastically increased by increasing the x-value. Fracture toughness moderately increased with x-value, although it was rather affected by local porosity. Elastic modulus showed a local minimal value at x ~ 0.3. Itakura et al. [42] attributed this V-shaped variation in elastic modulus with increasing Zr-content by using the first-principles calculation. They confirmed that disordering of O atoms in the fluorite structure is able to influence the elastic modulus as discussed in [42]. In the meantime, Takano et al. [43] studied the potential influence of B₄C coexistence in the fuel debris chemical status using surrogate materials. The mixture of (U,Zr)O₂, ZrO₂, Zr, SS and B₄C was synthesized by arc-melting and then the phase composition

was determined by XRD and SEM/EDX. Almost all of B and C were contained in the metal-rich region by forming borides (ZrB₂ or (Fe,Ni,Cr)₂B) and carbide (ZrC). The matrix of the metal-rich region consisted of a Fe-Cr-Ni solution phase and (Fe,Cr,Ni)Zr₂ and (Fe,Cr,Ni)₂(U,Zr) compounds. Furthermore, the TMI-2 debris samples stored at the JAEA hot cell were re-characterized (see Figure 15) [44]. These samples included two prototypic oxidic corium. The first one had been collected from the upper crust region which might have undergone fast cooling during the TMI-2 accident, whereas the other had been recovered from the molten pool region which could have been solidified under relatively slow cooling condition. Phase relation, microstructure, and micro hardness of these TMI-2 samples were compared with those obtained for surrogate materials in terms of cooling condition. The following similarities were identified as the common tendencies between the prototypic real oxidic corium and sim-debris synthesized in labo-scale tests:

- Quick cooling of the oxidic corium likely leads to form single phase with cubic structure (fluorite phase) as seen in the upper panels of Figure 16 (with the micro hardness value of 10.5–14 GPa) [44].

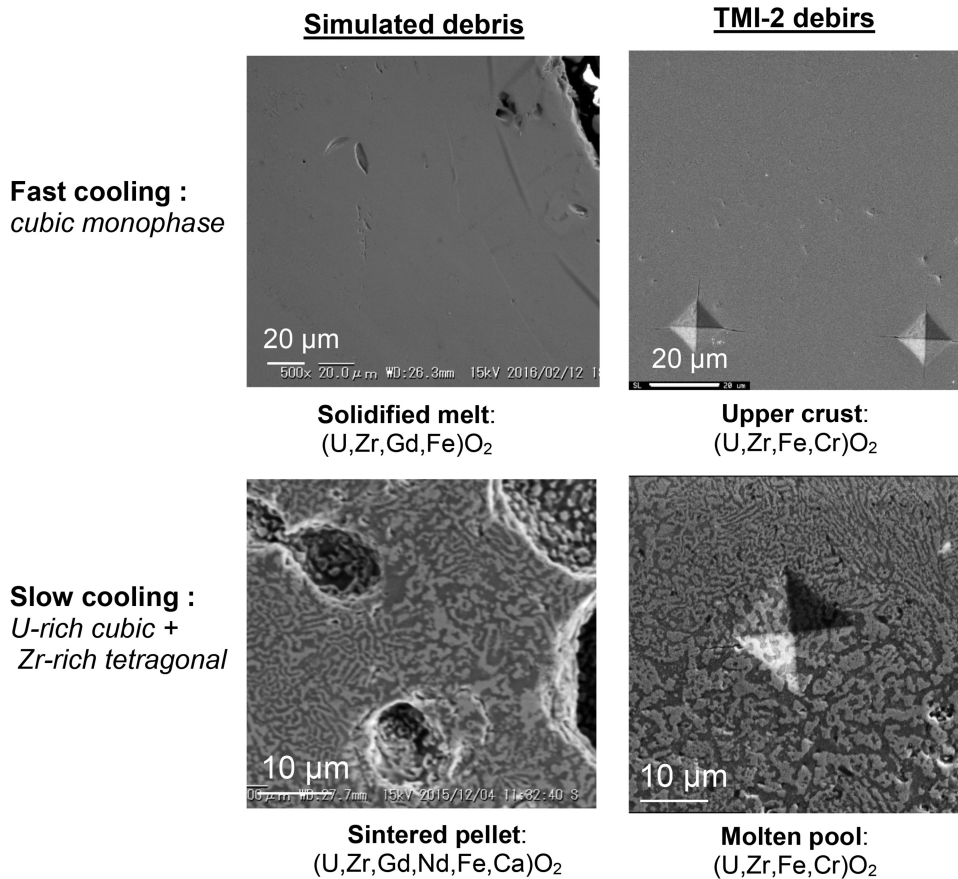


Figure 16. Microstructures observed in the oxide phases of the simulated, and the TMI-2 debris samples. Comparison at different cooling conditions [44].

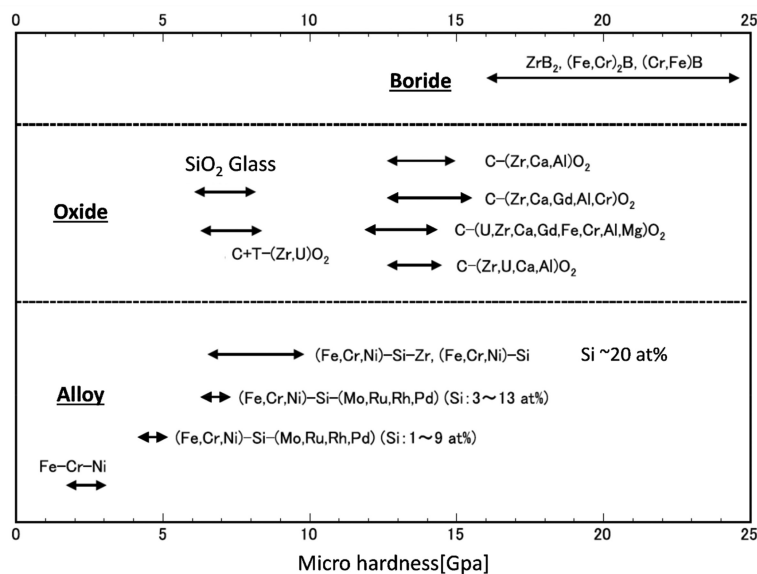


Figure 17. Micro-hardness of each phase detected in debris simulants [34]. C: cubic fluorite phase, T: tetragonal phase

- Slow cooling of the oxidic corium likely leads to form multiphase structure after solidification in which fine agglomerates of fluorite and tetragonal phases homogeneously coexist (see the lower panels of Figure 16 [44]). Fe-inclusion probably facilitates the phase separation in micron scale. Micro hardness ranges between 8 and 11 GPa.

Although the Pu-concentration in the fuel debris is rather small, the influence of Pu on the melting temperature of oxidic fuel debris was evaluated in a laboratory scale experiment (by a thermal arrest technique) [45]. It was found that the melting temperature of $(U,Pu,Zr)O_2$ solid solution is only slightly affected at concentrations below 20 mol% PuO_2 . However, it has a local minimum value of 2782 K with the PuO_2 -content between 0 and 20 mol%, in the condition that the molar ratio between UO_2 and ZrO_2 is almost 4:6. The $(U,Zr)O_2$ solid solution has a minimum melting point (~ 2830 K) at this molar ratio condition ($UO_2:ZrO_2 = 4:6$). Consequently, the melting temperature of ternary solution is approximately 50 K lower in maximum. The UO_2 - PuO_2 - ZrO_2 pseudo-ternary phase diagram in the temperature region between 2900 and 3000 K was drawn in [45] by comparing it to the previous data [46].

Based on these preliminary investigations [34,42–45], an important concern was pointed out for the mechanical property of the FDNPS fuel debris. According to literature survey and recent test results, Vickers hardness of the $(U,Zr)O_2$ base oxidic fuel debris increases with increasing the Zr-content. Furthermore, the coexistence of various borides, which could be formed from the interaction between structural materials or Zr-cladding/channel box and B_4C , with the oxidic fuel debris would physically

harden the fuel debris body (see Figure 17) [34]. The boride formation in the debris will lead to deterioration of the debris cutting tools (i.e. blade, drill, etc.) as discussed in [34].

Universities in Japan have also carried out vigorous R&D campaigns using surrogate materials, in which valuable knowledge has been gathered to characterize the FDNPS debris. Akiyama et al. [47,48] studied the fundamental interactions between UO_2 and various structural materials, such as cladding, control rod (B_4C , SS), and pedestal concrete (CaO , SiO_2), etc., under oxidizing and reducing conditions to confirm the chemical characteristics of the ex-vessel fuel debris. They identified $U(Fe,Cr)O_4$, $CaUO_4$ and U_3O_8 phases as oxides likely to be formed in the ex-vessel conditions as well as $(U,Zr)O_2$, in which the possible valence state of U is U^{4+} , U^{5+} or U^{6+} . Yusufu et al. [49] examined mechanical properties (e.g. Vickers hardness, Young's moduli, compressive strength) for UO_2 - B_2O_3 compounds for preliminary understanding of the influence of B-coexistence in the in-vessel fuel debris. The R&D groups of Osaka Univ. have comprehensively studied the mechanical and thermal properties (e.g. thermal conductivity, Vickers hardness, fracture toughness) for various alloys containing Fe, Zr and B (for metal-rich debris) and concrete materials (for ex-vessel debris) [50–52]. They concluded:

- Thermal conductivity of CrB and FeB is comparable to Fe_2B and therefore far smaller than that of ZrB_2 . On the other hand, Vickers hardness and fracture toughness of CrB and FeB are almost identical to each other and mostly similar to those of Fe_2B and ZrB_2 . Hence, thermal conductivity and Vickers hardness of the mixed borides are well estimated by the Effective Medium Theory (EMT) calculation;

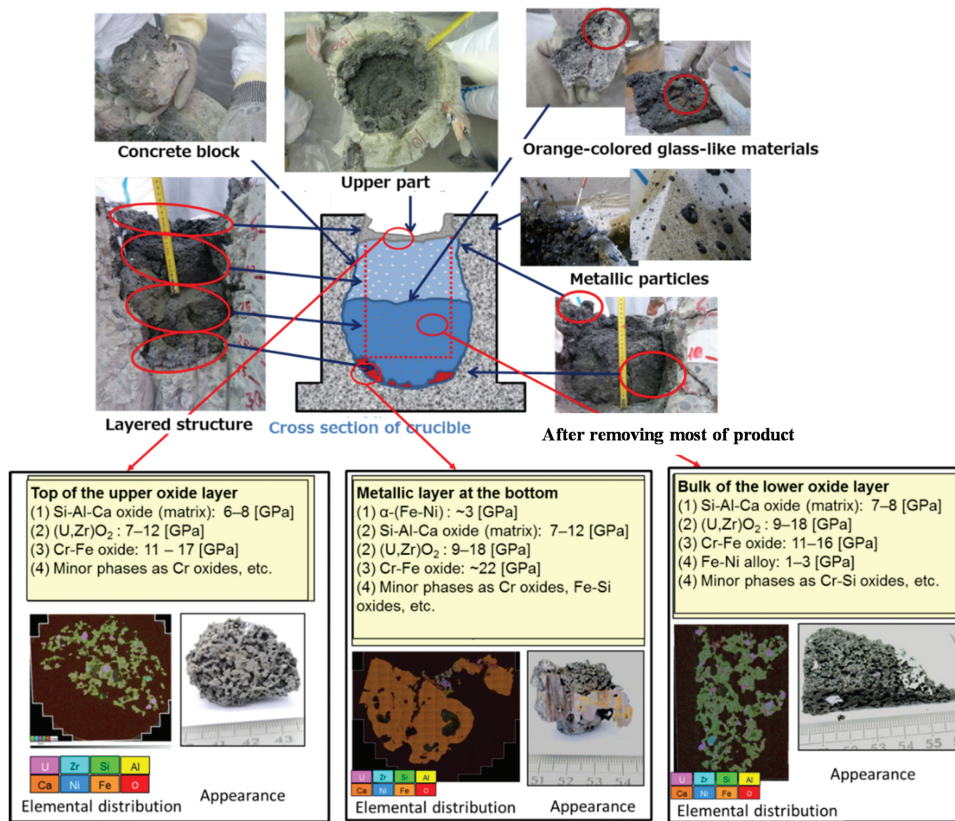


Figure 18. Appearance of large-scale MCCI experiment product [56,57].

- Thermal and mechanical properties of ZrSiO₄ have been determined: thermal conductivity (14.3 Wm⁻¹K⁻¹ at 298 K), Vickers hardness (17 ± 3 GPa) and fracture toughness (2.1 ± 0.5 MPa m^{1/2}).

Thermodynamic evaluations were performed in parallel to their experimental studies and then their original thermodynamic databases covering the U–Zr–Ce–Cs–Fe–B–C–I–O–H multicomponent system were developed as indicated in [53]. This database reflected their own assessment results as well as references to the conventional SGTE [54] and NUCLEA databases [55]. It enabled evaluating the phase equilibria in the fuel debris and volatilization behavior of FPs.

4-4 Characterization of ex-vessel debris at FDNPS

In the FDNPS accident, the interaction between molten fuel and concrete (MCCI: Molten core concrete interaction) might have occurred in the ex-vessel phase. Plenty of studies have been carried out so far on the post-test analysis of synthetic or realistic ex-vessel debris samples. However, as discussed above, we needed to improve our knowledge of the possible FDNPS conditions, especially BWR core materials (corium) interaction with basalt-base concrete. Hence, in addition to small-scale experiments using simulated debris, JAEA conducted a large-scale MCCI experiment under expected FDNPS conditions in cooperation with the French Alternative Energies and Atomic Energy

Commission (CEA: Commissariat à l'énergie atomique et aux énergies alternatives) including personnel detachments. The sim-MCCI experiment (~50 kg) was performed at the PLINIUS facility of the CEA Cadarache, and the generated products (using simulants including depleted UO₂) were analyzed by Vickers hardness, XRD, SEM/EDX, and ICP-MS in 2016–2017. Figure 18 shows the cross section of the sim-MCCI products obtained in this integral test [56,57]. The following results were obtained for characterizing the probable MCCI products at the FDNPS as discussed in [56,57]:

- The MCCI-melt was stratified into two regions; (i) metal-rich debris region rich in Fe and Ni deposited in an incomplete bottom layer of the melt, whereas (ii) oxidic debris region rich in (U,Zr,Fe)O₂ solidified as a main body, in which the pore-density is varied from place to place;
- The oxidic debris had Si-rich glassy matrix, in which small inclusions (a few to a few hundred microns in size) precipitated. These inclusions consisted of nodules of (U,Zr)O₂ phase and spinel-like (Fe,Cr)₃O₄;
- Vickers hardness varied from place to place depending on the dominant phases, in which the hardest were spinel-like oxides and the softest were the Fe-Ni base alloy. Vickers hardness of the oxidic debris matrix and nodular-shape precipitates varied between 7 and 12 GPa with location.

More importantly, the dismantling work of the large scale depleted UO_2 based debris conducted after the MCCI test indicated above gave us an important experience relevant to (i) selecting tools for hard debris cutting and handling, and also (ii) avoiding dust generation from the fuel debris cutting. This knowledge will be directly applied to the FDNPS decommissioning as discussed in [58]. Furthermore, the influence of the initial concrete composition and cooling conditions on the debris characteristics was also assessed by comparison with previous VULCANO MCCI tests, performed at CEA Cadarache mainly for Limestone-rich concrete [59]. The following features were identified:

- The interaction between molten corium and silica-rich concrete could likely form zircon phase containing a small amount of U, namely $(\text{Zr,U})\text{SiO}_4$, at the direct interface between corium and concrete [60];
- The rapid quenching (abrupt cooling) of MCCI-melt could form a significantly hardened material. The abrupt cooling is likely to occur at the top surface of ex-vessel corium melt (MCCI-melt). In these tests, it was caused by upward heat radiation losses, which could be caused by direct exposure of the corium surface to the injected cooling water in an accident [61].

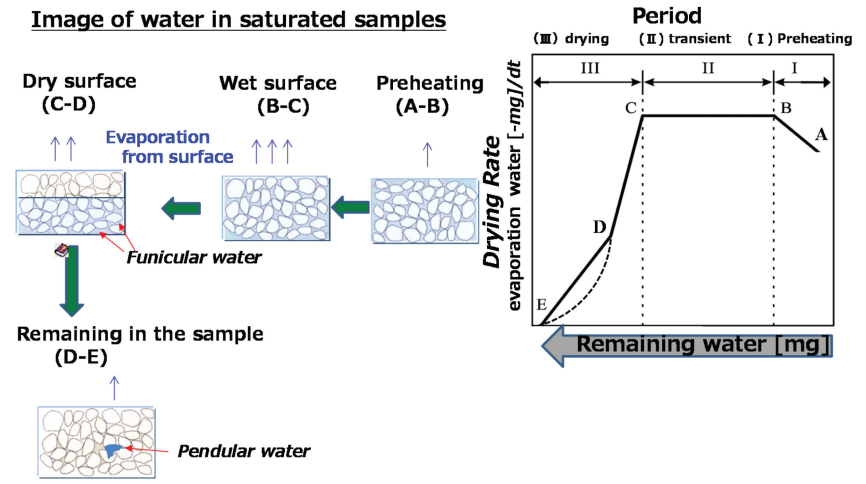
Also, the large-scale MCCI test samples demonstrated heterogeneous variation in material characteristics as discussed in [56,57]. The metal-rich layer could deposit at the bottom of the ex-vessel debris, presumably as the denser phase even if the metallic components were not fully oxidized. In the meantime, a significant amount of concrete materials could decompose and dissolve into the MCCI oxidic-melt and would be likely to decrease the oxidic-melt density. Much of the porosity observed in all phases is probably due to concrete decomposition (initial dehydration and then decarbonation of the concrete). The metal-rich deposit observed was likely to be ductile if the Zr-content is very low (due to Zr oxidation) and the phase was either scattered within the oxidic debris or was separated (as in the metal-rich bottom layer). A dispersion of softer material such as metal-rich debris may suggest that one needs to develop different debris retrieval tools or different cutting conditions for the locally difficult samples. As for the oxidic debris, the Si-rich glassy matrix is expected to be a dominant phase after a significant amount of concrete components (e.g. SiO_2 , Al_2O_3 , and CaO) have dissolved into the oxidic melt. This feature was also reported in small-scale experiments [62,63] as well as in lava samples collected from Chernobyl Unit 4 reactor

building [64]. Although these oxidic phases observed in the various ex-vessel debris samples were glassy and porous, the products contained inclusions and had become harder than the conventional glass materials.

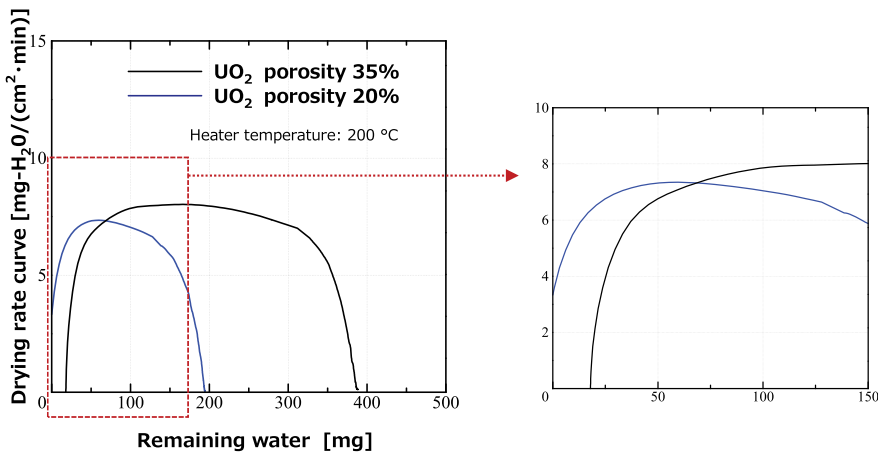
4-5 Feasibility studies for dust/aerosol treatment and debris storage

JAEA launched a new R&D in 2018 on the characteristics of simulated radioactive particles, which would be generated during the debris retrieval, in the cooperation with the ONET Technologies, CEA, and Institut de Radioprotection et de Sûreté Nucléaire (IRSN), France. Porcheron et al. [65] measured the size distributions and geometries of fine particles generated by cutting of two types of representative fuel debris simulant in the air and underwater conditions. These studies (using Hf and Ce to simulate U and Pu as well as non-radioactive FP elements mainly in oxidic phase) enabled the particulate composition and the particle size distribution of the prototypic aerosols to be established under these high power (and temperature) conditions as well as their aggregation/sedimentation behaviour. This is of great value for estimating the dispersion of contaminated particles in enclosed ventilated or non-ventilated spaces. This is essential basis for the assessment of the operators' radiation exposure risk.

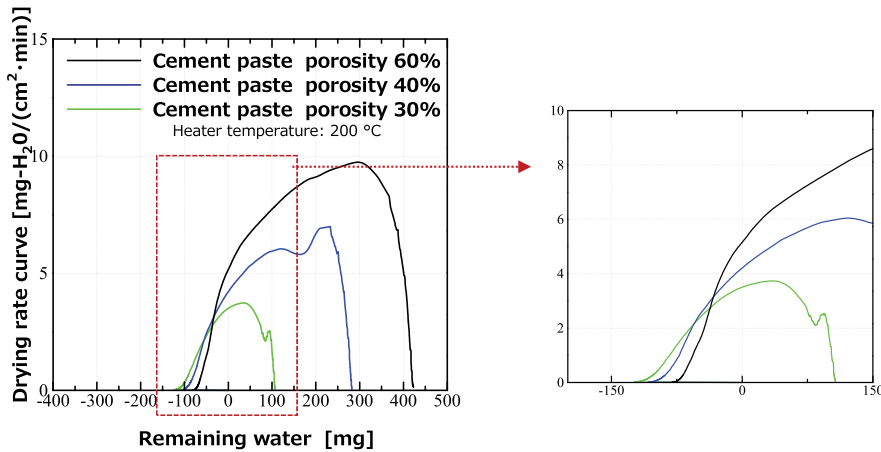
Regarding the medium- or long-term fuel debris management, several options are being discussed, including application of conventional fuel reprocessing technologies, debris conditioning or stabilization processes, container design, wet or dry storage and so on. For the fuel debris dry storage, the features of fuel debris drying will need to be recognized, because the fuel debris is immersed in water or kept in a very humid atmosphere before retrieval. Fuel debris drying with various geometries and porosities (particularly powder or porous lava-like types) will be necessary. In case of the porous fuel debris, 'how water captured in the pores evaporates depending on the pore's size within reasonable drying time' will be practically important. The drying rate curve analysis is generally employed to determine the drying characteristics of various materials [66], as indicated in Figure 19(a). In the prototypic condition, the weight change during drying is divided into three periods: 1) preheating, 2) transient, and 3) drying: At the beginning, the evaporation rate increases gradually with increasing temperature. Then, the water level lowers from the sample top in the transient period, in which the evaporation from the water surface and that from porosities or funicular water between pellets becomes dominant.



(a) Prototypic hysteresis of drying rate curve measurement [66]



(b) Drying rate curves of UO₂ pellets and enlargement for final stage [67]



(c) Drying rate curves of cement paste pellets and enlargement for final stage [68]

Figure 19. Drying rate curves of UO₂ and cement paste pellets. (a) Prototypic hysteresis of drying rate curve measurement [66]. (b) Drying rate curves of UO₂ pellets and enlargement for final stage [67]. (c) Drying rate curves of cement paste pellets and enlargement for final stage [67].

This results in mostly stable evaporation in the transient period. In the final drying period, the evaporation rate abruptly decreases than the transient period, since the evaporation from pendular water or porosities' inside becomes dominant.

Preliminary studies were carried out using pellet type samples of standard materials (e.g. UO₂, ZrO₂, cement paste, etc.) of known porosities to obtain the drying characteristics of these 'standard' oxide powders [67]. The pellet samples once immersed into

water (the porosities were then filled with water) was heated by an external heater (the temperature of the heat source was fixed to be 100 °C, 200 °C, 300 °C, and 1000 °C). The water level in the samples was gradually decreasing due to the evaporation of water and simultaneously the water amount in the porosities was decreasing. The weight change of the entire sample was continuously measured by a thermogravimetry. This enabled to evaluate the apparent drying rate of the pellet type samples, which were calculated from the weight change of water (mg) per unit time.

Figure 19(b) and (c) [67] show the drying curve of UO_2 and cement paste pellets, respectively. In case of UO_2 pellet with 20% or 35% porosities, the drying curve reasonably obeys the prototypic hysteresis from point-A to point-D. However, the hysteresis between point-D and point-E is not clearly observed. This suggests that the lower values of porosities do not significantly influence the final stage of drying. In case of cement paste pellets with 30% to 60% porosities, the decrease in the drying rate at the final stage (point-D to point-E) is clearly observed. In contrast, in the transient period (point-B to point-C), the drying rate is not constant and gradually decreasing. This might suggest that the evaporation from the porosities' inside becomes more dominant in the porous materials.

In contrast, when choosing wet storage, a fundamental dataset for long-term leaching is of primary importance. Static leaching experiments in aerated de-ionized water were carried out using in-vessel and ex-vessel debris simulant samples in the CEA Colima facility, in which oxidizing conditions by means of external gamma irradiation were applied [68]. The Fractional Release Rates of the $(\text{U,Zr})\text{O}_2$ matrix for the two kinds of samples (in-vessel and ex-vessel debris) were found to be close to (or one order of magnitude lower than) that of spent fuels under oxidizing conditions (from 10^{-6} to 10^{-7} per day). The Fraction of Inventory in Aqueous Phase (FIAP) of Mo, Ba, Sr, Rh, La, Nd, Ce and Y tended to be higher than that of U and Zr. The release of simulating FPs, including low volatile element like trivalent rare earth elements, did not appear to be fully controlled or associated with leaching processes of the $(\text{U,Zr})\text{O}_2$ matrix. One reason for this could be that the FPs could be partially located outside the $(\text{U,Zr})\text{O}_2$ solid solution phase. This, in turn, could be a function of the corium history (cooling rate and thermal history, chemical interactions ...). This behaviour parallels that of the spent fuel where the instant releases are observed of volatile FPs such as Cs or I that have already diffused to the grain boundaries [68]. In parallel, Kirishima et al. [69] performed leaching experiments using simulants for ex-vessel debris, in which the influence of Ca and Si in the leaching behaviour of the oxidic fuel debris was studied.

They found that Ca formed mixed oxides with ZrO_2 , UO_2 and $(\text{Zr,U})\text{O}_2$. In addition, CaO and SiO_2 in the debris tended to form a glassy coating that effectively suppressed the actinide leaching (^{237}Np and ^{241}Am as well as UO_2). Thus, differences in leaching mechanisms are to be expected in the ex-vessel debris formed by MCC1. Finally, aqueous/pyro reprocessing techniques were preliminarily investigated for their feasibility to treat fuel debris, particularly for concrete components (e.g. high SiO_2 content material) [70].

4-6 Issues relevant to fuel debris analyses

In the present section, the issues relevant to real fuel debris analyses, which will be essentially unknown (with various sizes and characteristics), are discussed in terms of practical analysis manner.

(1) Essential features of the FDNPS debris and previous experiences on the debris analyses

The fuel debris generated in the FDNPS accident will have the following essential features:

- The debris contains an extremely large number of elements or nuclides with various origins, i.e. (i) core materials including fuel, core components and FPs, (ii) structural materials including steels and (iii) building materials: concrete, insulator, shielding, paint and etc., and (iv) seawater or other biological or environmental components;
- The debris is likely composed of multiple regions, phases and elements. The proportions of them can be widely scattered from place to place in PCV or RPV and also scattered in scale: meso-scale (μm to cm) or macroscale (several tens of cm or larger);
- The debris will have various forms, i.e. massive or porous stone, plate, fragment, wet particles, dry powder, aqueous sediments or suspensions, stump-like remaining fuel assembly, etc. Some of them may have different physical characteristics such as being large and hard and therefore difficult to cut, or very fine particles that disperse easily. Alternatively, they may have extreme chemical characteristics: being difficult to dissolve in acid (and therefore difficult to analyze by aqueous analytical methods) or being extremely reactive and volatile (and therefore awkward to accurately predict).

Hence, one must recognize that the fuel debris at the FDNPS is an extremely diverse sample as a prerequisite for establishing the analytical technology. Much experience in the debris analysis has already been collected by national laboratories that have participated in the analysis for TMI-2 or Chernobyl debris samples or in-pile test samples

such as Phébus FP. First, they had established a succession of simple preliminary techniques suitable for checking many samples (non-destructive, simple and rapid techniques). Then, they had moved forward to slower, time-consuming but more accurate (and usually destructive) techniques on fewer samples. Finally, very specialized and mostly time-consuming techniques were applied to a few key samples for the most accurate and essential measurements (e.g. actinide isotopic composition, neutron interrogation). These features will benefit from the latest improvements, especially automated analyses and those developed for spent nuclear fuels.

(2) Analysis method for ‘unknown’ fuel debris samples

While referring to this previous knowledge, JAEA started discussing the following issues for the FDNPS debris analysis in collaboration with TEPCO experts [71]. A practically important issue to be discussed for the FDNPS fuel debris analyses is that we need to treat ‘unknown’ fuel debris samples in hot cells. To improve efficient qualitative analysis of fuel debris samples, the use of X-ray computer tomography (CT) technology (used in Phébus FP) is being discussed to assess the porosity distribution within large samples. In many cases, the bulk of the massive fuel debris can have different features from the surface and hence the development of suitably accurate cutting equipment also needs to be developed.

The multi-nuclide analysis by ICP-MS will be a major method for the chemical analysis; this needs the establishment of peak overlap database as well as the use of supplementary (pre- and post-MS) techniques to enhance the possibilities of isotopic analysis and to maintain the quantitative accuracy and level of calibration to avoid misinterpretation (the application of ICP-MS to extremely multi-element samples is still a big challenge). Regarding the dissolution technology for very poorly soluble materials such as Zr-based or Si-based oxides, the use of aqua regia or an addition of hydrofluoric acid to nitric acid is being discussed and the experiences from previous tests (e.g. TMI-2 or Phebus FP) were also examined. These techniques are being validated using the FDNPS samples and surrogate materials in JAEA [32,71]. In the meantime, JAEA is also examining an alkali fusion method especially for dissolving the ex-vessel debris

containing concrete materials [32,71]. However, these Zr-based and Si-based mixed oxides are the most insoluble materials in chemistry. One needs to further discuss on back-up spectroscopic methods to analyze the residues from the wet chemical analysis. Establishing the improved analysis flow will be particularly important when making declarations of barrels of material for storage.

Samples collected in the early stage of the debris retrieval will be extremely valuable and analysis need to be carried out as completely as possible to meet decommissioning requirements. For example, recriticality evaluation is inevitably important for designing the debris retrieval process, which requires the accurate concentration of U, Pu, other actinides, Gd, and other neutron absorbers and distribution of these elements, isotopic ratio etc. This requires the expert combination of various analysis techniques, including chemical analysis (e.g. ICP-MS, ICP-AES, etc.), microscopic analysis (SEM/EDX, SEM/WDX, TEM, etc.), and radiation analysis (α/γ -spectrometry, neutron measurement, etc.) by laboratories that have analytical specialists to ensure best practice and standards. JAEA has already published a report in 2020 [71], in which the decommissioning requirements and fuel debris properties to be analyzed are comprehensively discussed. The contents have been reviewed by the international experts in the OECD/NEA PreADES project (see chapter 5). This will be a fundamental knowledge base for establishing the analytical flow for the debris samples. Currently, the first debris retrieval is roughly estimated to be more or less a few gram. The detailed analysis plan is being discussed in JAEA and IRID [32], in which the SEM/EDX or SEM/WDX will be used firstly for the outline analysis of gram-size samples.

(3) Representativeness of ‘massive’ debris samples

In parallel, another important practical issue is the representativeness of the ‘massive’ debris samples. In order to facilitate the discussion efficiently, we would like to introduce the following key concepts:

- The analysis is done on ‘micro-scale’ or ‘analytical-scale’ (typically, ~ 1 mg or less in chemical analysis or ~ 100 μm square or less in microscopic analysis) to determine the composition of the gram-size ‘mesoscale’ regions in the debris samples;

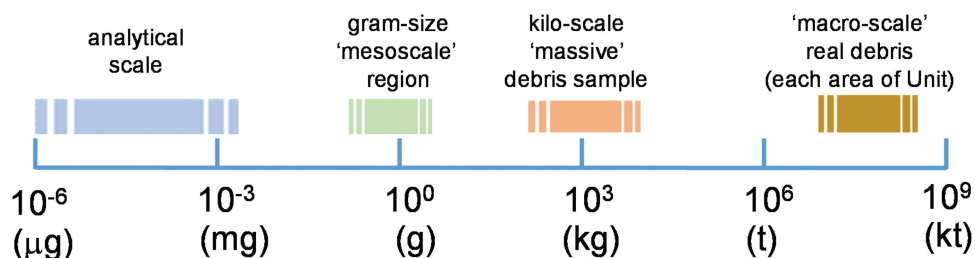


Figure 20. Typical scales for debris sample analysis.

- These 'mesoscale' regions are extracted from the fuel debris samples removed from the FDNPS site on the 'kilo-scale' (typically, 100 g ~ a few kg);
- From the 'limited' information obtained from the debris sample analyses, we need to estimate the overall distribution and characteristics of core materials and the interaction with various materials on the 'macro-scale' (>1000 kg) in each area at a reactor site.

Considering the current debris retrieval plan at the FDNPS, the significant problem is to estimate the best 'macro-scale' compositions and other characteristics (overall material distribution) from the optimized 'kilo-scale' compositions and other characteristics. This 'kilo-scale' estimation also needs to take into account the assumptions (and error margins) made for 'mesoscale' region compositions and other characteristics, which are evaluated from directly measured 'micro-scale' analyses data. Figure 20 illustrates the relations of typical scales for the debris analysis.

Consequently, the following two aspects are pointed out in terms of representativeness:

- [Analysis of heterogeneous 'kilo-scale' debris sample] How best to evaluate the 'average or optimized' properties and the error margin of 'kilo-scale' debris sample, using the analysis data for 'spots (i.e. mesoscale data evaluated from the analytical scale measurement)';
- [Best prediction of overall debris distribution from 'local optimized' data] How best to evaluate the area distribution of the 'fuel debris body' and any accompanying structural materials of the PCV or RPV inside, using the 'local optimized' analysis results of the 'kilo-scale' debris samples (described above); in other words, methods for evaluating how representative the collected 'kilo-scale' debris samples compared to the overall properties of the accumulated 'fuel debris body' (probably widely scattered in characteristics from place to place).

Regarding the first aspect, there is no almighty analysis methods but we need steady progress in qualitative analysis to identify elements or nuclides, then confirm and extend this with further, suitable quantitative analysis methods for the various spots in the 'kilo-scale' samples by means of conventional analytical techniques. Previous experience gained from TMI-2, Chernobyl and various in-pile tests will be very valuable. The quantitative analysis will also have a confidence limits (error evaluation) and will identify analysis problems (e.g. mass balance in 'kilo-scale' samples, peak overlap in 'spots'). In addition, it is highly necessary to record and store these collection data, location of spots, these analysis processes, judgment

grounds, and process of correction. This is the so-called 'quality assurance' of the fuel debris analysis. JAEA has just started establishing a practical methodology based on the analysis of lava samples in geology.

The second aspect is 'how representative is the existing debris sample analysis to the overall "fuel debris body"?' Currently, several types of fuel debris have been found in the inside of the PCV that have very different appearances (perhaps different characteristics as well). It is clear that the proportions of these different types of debris will vary with location of the PCV and/or RPV inside according to the local conditions causing relocation from above. Chernobyl lava had also shown the variation in morphologies according to location. Therefore, from the initial stage of retrieval, we need to store and classify the data as the results are accumulated and to compare the characteristics from analysis with the a) location (original fixed position or position lying on floor) and b) appearance (detailed visual retrieval data) of local fuel debris. The continued evaluation of the results will enable the improvement of mapping and composition/distribution estimates of major fuel debris domains. Comparison with the inventory will indicate the compositions of the remaining fuel debris. Accident modelling analysis for debris location/accumulation/characteristics will also assist identifying data gaps and indicate supplementary or verification data to be obtained by out-of-pile tests if necessary. Continuous cross-expert discussions will be necessary during the progress of debris retrieval.

5. International collaboration at OECD/NEA

In the OECD/NEA [72], there are seven committees under the steering committee for nuclear energy. The FDNPS-issues relevant to the decommissioning and accident analysis have been discussed and investigated mainly in two committees, i.e. Committee on the Safety of Nuclear Installations (CSNI) and Nuclear Science Committee (NSC). The issues relevant to the waste management will be separately discussed in Radioactive Waste Management Committee (RWMC). In Chapter 5, the major activities in CSNI and NSC at the OECD/NEA for the post-FDNPS period are outlined.

In June 2013, the Senior Expert Group on Safety Research Opportunities Post-Fukushima (SAREF) was launched in CSNI for identifying the gap between the issues that became apparent in the FDNPS accident and the current technology level. The committee then properly promoted safety research in support of the FDNPS decommissioning. Discussions were held on: (i) what kind of R&D activities were to be carried out based on the knowledge obtained in the modelling analysis of the accident to support the decommissioning and (ii) how to provide the NEA member

countries with newly obtained knowledge on nuclear safety. The summary report was published in 2016 [73], describing near-term and long-term R&D subjects. The near-term R&Ds were defined as necessary in the preparatory phases (see Introduction, for Phase 1 and Phase 2 of the decommissioning roadmap), whereas the long-term corresponds to the Phase 3. After the preliminary meeting for the near-term issues in January 2017, two such projects were launched in CSNI, i.e. Preparatory Study on Analysis of Fuel Debris (PreADES) [74] and Analysis of Information from Reactor Buildings and Containment Vessels of Fukushima-Daiichi Nuclear Power Station (ARC-F) [75]. The PreADES is mainly focusing on the characteristics of the fuel debris and whereas ARC-F is focusing on maximizing the safety knowledge derived from the FDNPS sample analysis. The accident modelling analysis (from the BSAF/BSAF2 projects in the NEA (see below)) is being continued in ARC-F. The status of the FDNPS fuel debris evaluated in the PreADES project was reported in [76].

One important issue that arose just after the FDNPS accident was analysis using severe accident analysis codes (SA-codes). Many organizations had attempted the accident analysis for three units of the FDNPS using various SA-codes, including MAAP, MELCOR, ASTEC, THALES-2, SAMPSON, and SOCRAT. In 2012, just prior to SAREF formation, at the call of the NEA, a Benchmark Study of the Accident at the Fukushima-Daiichi Nuclear Power Station (BSAF) was started [77]. In the phase 1 of the BSAF project, an analysis was conducted focusing on the transition of the thermal-hydraulic state of the RPV and PCV insides for six days after the loss of DC power. The analysis results were compared to each other. Then, the analysis was taken over by the phase 2 (BSAF2), in which the analyzed period was expanded to three weeks after the accident. The BSAF2 was successfully completed in 2019.

Meanwhile, the Ministry of Education, Culture, Sports, Science and Technology (MEXT) of Japan proposed to the NEA the acceleration of R&Ds relevant to the FDNPS decommissioning by the efficient contribution of scientists and researchers for the fundamental R&D fields in December 2016. Then, Thermodynamic Characterization of Fuel Debris and Fission Products based on Scenario Analysis of Severe Accident Progression at Fukushima-Daiichi Nuclear Power Station (TCOFF) project [78] was launched by the NSC. In the TCOFF project, R&D issues related to the fuel debris and FP were discussed through synergies involving not only nuclear safety research experts but also fundamental science specialists who may not have been directly involved in the nuclear safety research. The obtained materials science knowledge was provided for PreADES,

ARC-F and domestic R&Ds in Japan, including improved thermodynamic knowledge for the fuel debris and FP, corium behaviour in terms of material interaction or reaction, and leaching data from fuel debris. The TCOFF final report will be published by end 2021 [79].

6. Summary

There are still many unclear points, but a survey of previous experiences such as TMI-2 decommissioning and in-pile testing, investigations of the inside of the PCV and R/B, sample analysis, various sim-tests, accident modelling analysis, etc. has been carried out. As a result, the debris characteristics and distribution at the PCV bottom (so-called ex-vessel debris) and the damage status of the inside of the PCV has been improved, step by step for the three units. Based on the knowledge and data obtained so far, the accumulated debris status and characteristics of each unit, as well as the damage status of the inside of the PCV, have the following features:

Unit 1: Interactions between molten core materials and concrete have happened. The surface of ex-vessel debris was presumably covered with sediment (the origin is likely to be concrete products with a small amount of steel). Presumably, a considerable amount of ex-vessel debris has spread out of the RPV pedestal region to the D/W region.

Unit 2: A significant amount of fuel debris still exists in the RPV (likely to be in the lower part). Two debris relocation paths were identified: (i) through a large breach at the side wall of the RPV lower head, a significant amount of the fuel debris (probably rich in metallic components) relocated to the RPV pedestal region in a short time, (ii) through several small breaches at the vulnerable part of the RPV bottom, a small amount of the fuel debris (likely to be rich in oxidic debris) penetrated and fell down to the pedestal region. According to the limited damage status of steel and concrete materials which were originally positioned in the RPV pedestal, the interaction between the fuel debris and these structural materials is expected to be rather limited.

Unit 3: The RPV bottom was severely damaged and a huge amount of the fuel debris accumulated in the RPV pedestal with damaged steel materials. The appearance of the accumulated materials indicates that the fuel debris had gradually relocated from the RPV to the pedestal probably for a few hours. Furthermore, the debris temperature during relocation is considered to be rather lower than the

fully liquefied temperature. This might indicate that MCCI may not be very significant in Unit 3. Vacancies or cavities could exist in the inside of the ex-vessel debris. A considerable amount of the fuel debris is still likely to exist in the RPV.

As such debris characterization and core status analysis progresses, several important issues have been identified and studied for the debris retrieval and analysis in the near future:

- Regarding the fuel debris retrieval, various practical problems for the retrieval require a solution, including dust/aerosol dispersion, debris drying, long-term leaching and debris processing (if necessary);
- Regarding the fuel debris analyses, improvement of analytical techniques is still highly necessary based on various requirements of decommissioning, including sample preparation techniques for as yet poorly characterized materials (although previous experiences for TMI-2, Chernobyl and in-pile tests are very helpful);
- Establishment of quality assurance method and maintaining an updated database, including analysis flow and traceability is necessary. Development of an evaluation method for the debris representativeness is of particular importance in the trial stage of fuel debris retrieval.

There is no almighty analysis method that can satisfy all issues. It is unlikely that the information and data finally needed for decommissioning requirements will be comprehensively obtained only by analyzing the debris samples (especially, in the early phase of the debris retrieval and the analysis). A step-by-step progress in analysis and debris characterization along with a FDNPS forensic investigation approach will be necessary. This will utilize not only debris sample analysis data but various relevant knowledges from site monitoring and operation data, including the collaboration with international experts and their facilities, across wide ranges of R&D fields and generations of scientists.

Acknowledgments

This paper includes results obtained under the research program entrusted to the International Research Institute for Nuclear Decommissioning, including the Japan Atomic Energy Agency, sponsored by the Agency for Natural Resources and Energy, Ministry of Economy, Trade and Industry (METI) of Japan. JAEA and IRID colleagues who contributed to the relevant R&D projects (Drs. T. Washiya, T. Mitsugi, H. Madokoro, H. Ohgi, A. Pshenichnikov, T. Ohnishi and D. Bottomley and Mrs I. Sato, T. Yamashita, T. Sato, H. Hirano and S. Sasaki (JAEA) and Mr K. Takamori and Mr T. Ohashi (IRID)) are gratefully acknowledged. Also, the authors wish to express their appreciation to Drs

S. Mizokami, M. Hirai, and K. Ito and Mr M. Mizokami of TEPCO and Dr A. Suzuki of NFD for the fruitful discussions regarding sample analysis and core status evaluation.

Disclosure statement

No potential conflict of interest was reported by the author(s).

References

- [1] Statement of the Nuclear Emergency Response Headquarters. Japanese. Available from: <https://www.meti.go.jp/earthquake/nuclear/pdf/111216a.pdf>
- [2] Nuclear Emergency Response Headquarters Council for the decommissioning of TEPCO's Fukushima Daiichi Nuclear Power Station, Mid-and-Long-Term Roadmap towards the Decommissioning of TEPCO's Fukushima Daiichi Nuclear Power Station Units 1-4, 2013 Jun 27. Recently revised in December 27, 2019, by The Inter-Ministerial Council for Contaminated Water and Decommissioning Issues. Available from: https://www.meti.go.jp/english/earthquake/nuclear/decommissioning/pdf/20191227_3.pdf
- [3] Position statement of Atomic Energy Society of Japan. Japanese. Available from: <https://www.aesj.net/document/aesj-ps022.pdf>
- [4] The Project of Decommissioning and Contaminated Water Management. Available from: <https://en.dccc-program.jp/>
- [5] International Research Institute for Nuclear Decommissioning. Available from: <https://irid.or.jp/en/research/>
- [6] Yamashita T, Sato I, Honda T, et al. Comprehensive analysis and evaluation of Fukushima Daiichi Nuclear Power Station Unit 2. Nucl Technol. 2020;206(10):1517–1537.
- [7] Published movie by Tokyo Electric Power Corporation. Japanese. Available from: https://www.tepco.co.jp/library/movie/detail-j.html?catid=61709&video_uuid=m88yqm90
- [8] Core status map of Fukushima Daiichi Nuclear Power Station, presented in debrisWiki. Japanese. Available from: <https://fdada-plus.info/wiki/index.php?title=%E7%82%89%E5%86%85%E7%8A%B6%E6%B3%81%E6%8E%A8%E5%AE%9A%E5%9B%B3#.E6.83.85.E5.A0.B1.E9.9B.86.E7.B4.84.E5.9B.B3>
- [9] International Research Institute for Nuclear Decommissioning. Available from: https://irid.or.jp/_pdf/pamphleth27_eng.pdf?v=2
- [10] Tokyo Electric Power Corporation. Available from: https://www.tepco.co.jp/decommission/common/images/progress/retrieval/unit1_meeting_20150430.pdf
- [11] International Research Institute for Nuclear Decommissioning. Available from: https://irid.or.jp/_pdf/IRID_robots2019_eng.pdf
- [12] International Research Institute for Nuclear Decommissioning. Available from: https://irid.or.jp/_pdf/1_Development%20of%20Detailed%20Investigation%20inside%20PCV_IRID_2019.pdf
- [13] Tokyo Electric Power Corporation. Japanese. Available from: https://www.tepco.co.jp/nu/fukushima-np/handouts/2018/images2/handouts_180810_04-j.pdf

- [14] Ministry of Trade and Industry, Japan. Japanese. Available from: <https://www.meti.go.jp/earthquake/nuclear/decommissioning/committee/osensuitaisaku/team/2019/04/3-4-3.pdf>
- [15] International Research Institute for Nuclear Decommissioning. Available from: https://irid.or.jp/_pdf/pamphleth28_eng.pdf
- [16] International Research Institute for Nuclear Decommissioning. Available from: https://irid.or.jp/_pdf/pamphleth29_eng.pdf
- [17] International Research Institute for Nuclear Decommissioning. Available from: https://irid.or.jp/_pdf/pamphleth30_eng.pdf
- [18] Tokyo Electric Power Corporation. Available from: https://www.tepco.co.jp/decommission/common/images/progress/retrieval/unit2_meeting_20190228.pdf
- [19] Pshenichnikov A, Kurata M, Nagae YA. Comparison of the observed Fukushima Dai-Ichi Unit 2 debris with simulated debris from the CLADS-MADE-01 control blade degradation test. *J Nucl Sci Technol.* 2021;58(4):418–425.
- [20] Pshenichnikov A, Yamazaki S, Bottomley D, et al. Features of a control blade degradation observed in situ during severe accident conditions in boiling water reactors. *J Nucl Sci Technol.* 2019;56(5):440–453.
- [21] Pshenichnikov A, Nagae Y, Kurata M. On the degradation progression of a BWR control blade under high-temperature steam-starved conditions. *Mech Eng J.* 2020;7(3):1–10.
- [22] Pshenichnikov A, Kurata M, Nagae Y, et al. The behaviour of materials in case of solidified absorber melt - oxidized BWR channel box interaction revealed after CLADS-MADE-01 test. Proceedings of the International Topical Workshop on Fukushima Decommissioning Research (FDR2019); 2019 May 24–26; Naraha, Fukushima, Japan, (Paper No. FDR2019-1058).
- [23] Pshenichnikov A, Yamazaki S, Nagae Y, et al. Heterogeneity of BWR control blade degradation under steam-starved conditions. Proceedings of ICONE 27 the 27th International Conference on Nuclear Engineering; 2019 May 19-24; Ibaraki, Japan, (Paper No. ICONE27-1077).
- [24] Tokyo Electric Power Corporation. Available from: http://www.tepco.co.jp/en/nu/fukushima-np/handouts/2018/images/handouts_180426_03-e.pdf
- [25] Bottomley D, Coquerelle M. Metallurgical examination of bore samples from the Three Mile Island Unit 2 reactor core. *Nucl Technol.* 1989;87(1):120–136.
- [26] International Research Institute for Nuclear Decommissioning. Available from: https://irid.or.jp/wp-content/uploads/2020/08/pamphleth31_eng.pdf
- [27] Japan Atomic Energy Agency, debrisWiki. Japanese. Available from: <https://fdada-plus.info>
- [28] Barrachin M, Nakayoshi A, Kurata M, et al. Preliminary investigation of samples taken from the PCV inside of Fukushima-Daiichi Nuclear Power Plant and implications on severe accident analysis. Proceedings of the 19th International Meeting on Nuclear Reactor Thermal Hydraulics (NURETH19), 2022 March 6–11; Brussels (Belgium). (to be published.)
- [29] Mizokami S. Current status and recent investigation result of Fukushima Daiichi, presented in the plenary session, ERMSAR2019, Prague, Czech Republic, March 2019.
- [30] Nishihara K, Iwamoto D, Suyama K, Evaluation of fuel composition of Fukushima-Daiichi Nuclear Power Station. JAEA-Data/Code 2012-018. Japanese.
- [31] Grambow B, and Poinssot, C. Interactions between nuclear fuel and water at the Fukushima Daiichi Reactors. DOI: 10.2113/gselements.8.3.213
- [32] International Research Institute for Nuclear Decommissioning, Development of technology for fuel debris analysis and characterization interim report. April 2018. https://irid.or.jp/_pdf/4_Development%20of%20Technology%20for%20Fuel%20Debris%20Analysis%20and%20Characterization%20_IRID_2019.pdf
- [33] Japan Atomic Energy Agency, Fuel debris characterization and treatment technologies development for TEPCO's Fukushima Daiichi Nuclear Power Station –2012 annual research & development report, Fuel Debris Conditioning Technology Development Group, JAEA-Review 2013-066, 2013. Japanese.
- [34] Yano K, Kitagaki T, Ikeuchi H, et al. Direction on characterization of fuel debris for defueling process in Fukushima Daiichi Nuclear Power Station. Proceedings of International Nuclear Fuel Cycle Conference (GLOBAL2013); 2013 Sep 29-Oct 3; Salt Lake City (USA). [CD-ROM].
- [35] Bale CW, Bélisle E, Chartrand P, et al. FactSage thermochemical software and databases, 2010–2016. *CALPHAD.* 2016;54:35–53.
- [36] Cheynet B. NUCLEA Nuclear Thermodynamic Database Version 2005-01 2005. 79 pages.
- [37] Ikeuchi H, Yano K, Kaji N, et al. Suggestion of typical phases of in-vessel fuel-debris by thermodynamic calculation for decommissioning technology of Fukushima-Daiichi Nuclear Power Station. Proceedings of International Nuclear Fuel Cycle Conference (GLOBAL2013); 2013 Sep 29-Oct 3; Salt Lake City (USA). [CD-ROM].
- [38] Kitagaki T, Yano K, Ogino H, et al. Thermodynamic evaluation of the solidification phase of molten core-concrete under estimated Fukushima Daiichi Nuclear Power Plant accident conditions. *J Nucl Mat.* 2017;486:206–215.
- [39] Ishikawa J, Yonomoto T, Maruyama Y THALES2 code analysis on transient behavior during Fukushima Dai-ichi NPP accident. Proceedings of the 2012 Fall Meeting of the Atomic Energy Society of Japan; 2012 Sep 19-21; Higashi-Hiroshima, Japan. M1. Japanese.
- [40] Hoshino T, Kitagaki T, Yano K, et al. Mechanical properties of fuel debris for defueling toward decommissioning. Proceedings of the 23rd International Conference on Nuclear Engineering (ICONE 23); 2015 May 17-21; Chiba, Japan. [DVD-ROM].
- [41] Kitagaki T, Hoshino T, Yano K, et al. Mechanical properties of cubic (U,Zr)O₂. *J Nucl Eng Rad Sci.* 2018;4(3):031011.
- [42] Itakura M, Nakamura H, Kitagaki T, et al. First-principles calculation of mechanical properties of simulated debris Zr_xU_{1-x}O₂. *J Nucl Sci Technol.* 2019;56(9–10):915–921.
- [43] Takano M, Nishi T, Shirasu N. Characterization of solidified melt among materials of UO₂ fuel and B₄C control blade. *J Nucl Sci Technol.* 2014;51(7–8):859–875.

- [44] Takano M, Onozawa A, Suzuki M, et al. Revisiting the TMI-2 core melt specimens to verify the simulated corium for Fukushima Daiichi NPS. Proceedings of HOTLAB 2017; 2017 Sep 17-22; Mito, Japan.
- [45] Morimoto K, Hirooka S, Akashi M, et al. The influences of Pu and Zr on the melting temperatures of the UO_2 - PuO_2 - ZrO_2 Pseudo-Ternary System. *J Nucl Sci Technol.* 2015;52(10):1247–1252.
- [46] Lambertson WA, Mueller MH. Uranium oxide phase equilibrium systems: III, UO_2 - ZrO_2 . *J Am Ceramic Soc.* 1953;36(11):365–368.
- [47] Akiyama D, Akiyama H, Kirishima A, et al. Reaction behavior of uranium oxides and structural materials at high temperatures. Proceedings of the International Nuclear Fuel Cycle Conference (GLOBAL2015); 2015 Sep 20-24; Paris, France.
- [48] Akiyama D, Akiyama H, Uehara A, et al. Phase analysis of uranium oxides after reaction with stainless steel components and ZrO_2 at high temperature by XRD, XAFS, and SEM/EDX. *J Nucl Mat.* 2019 Apr;520:27–33.
- [49] Yusufu A, Uno M. Microstructure and mechanical properties of eutectic B_2O_3 - UO_2 ceramic composites solidified at different cooling rates. *J Nucl Mat.* 2017 Nov;499:175–181.
- [50] Nakamori F, Ohishi Y, Muta H, et al. Mechanical and thermal properties of ZrSiO_4 . *J Nucl Sci Technol.* 2017 Aug;54(11):1267–1273.
- [51] Ohishi Y, Sugizaki M, Sun Y, et al. Thermophysical and mechanical properties of CrB and FeB. *J Nucl Sci Technol.* 2019 Mar;56(9–10):89–865.
- [52] Sun Y, Abe Y, Muta H, et al. Mechanical and thermal properties of Zr-B and Fe-B alloys. *J Nucl Sci Technol.* 2020 Mar;57(8):8 917–925.
- [53] Suzuki M, Kurosaki K, Yamanaka S, et al. Development of thermodynamic databases in the system U–Zr–Ce–Cs–Fe–B–C–I–O–H for application to simulating phase equilibria in severe nuclear accidents. *J Nucl Sci Technol.* 2018 Mar;55(8):8 885–899.
- [54] SGTE – scientific Group Thermodata Europe. Available from: <http://www.sgte.net>
- [55] Chevalier P-Y, Cheynet B, Fischer E. Chapter II. Interpretation of complex thermochemical phenomena in severe nuclear accidents using a thermodynamic approach. In: The SGTE casebook. 2 ed. Cambridge: Woodhead Publishing Ltd; 2008. p. 161–177.
- [56] Brissonneau L, Ikeuchi H, Piluso P, et al. Material characterization of the VULCANO corium concrete interaction test with concrete representative of Fukushima Daiichi Nuclear Plants. *J Nucl Mat.* 2019 Oct;528:151860.
- [57] Bouyer V, Journeau C, Haquet JF, et al. Large scale VULCANO molten core concrete interaction test considering Fukushima Daiichi condition. Proceedings of the 9th European Review Meeting on Severe Accident Research (ERMSAR2019); 2019 March 18-20; Prague (Czech Republic).
- [58] Nakayoshi A, Ikeuchi H, Kitagaki T, et al. Knowledge obtained from dismantling of large-scale MCCI experiment products for decommissioning of Fukushima Daiichi Nuclear Power Station. Proceedings of the International Topical Workshop on Fukushima Decommissioning Research; 2019 May 24-26; Naraha (Japan).
- [59] Brissonneau L, Journeau C, Piluso P, et al. Prototypic corium analysis: a round robin for SEM and EDS characterization. *Mater Sci Eng.* 2012;32:012005.
- [60] Kitagaki T, Ikeuchi H, Yano K, et al. Characterization of the VULCANO test products for fuel debris removal from the Fukushima Daiichi Nuclear Power Plant. *Prog Nucl Sci Technol.* 2018;5:217–220.
- [61] Kitagaki T, Ikeuchi H, Yano K, et al. Effect of quenching on molten core-concrete interaction product. *J Nucl Sci Technol.* 2019;56(9–10):902–914.
- [62] Sudo A, Takano M, Onozawa A Characterization of core melt/concrete interface region examined by light-concentrating heating technique, presented as NUMAT-2016, Montpellier, France 2016 Nov 7-10.
- [63] Sudo A, Sato T, Ohgi H, et al. Experimental evaluation of Sr and Ba distribution in ex-vessel debris under a temperature gradient. *J Nucl Sci Technol.* 2021;58(4):473–481.
- [64] Shiryayev AA, Vlasova IE, Burakov BE, et al. Physico-chemical properties of Chernobyl lava and their destruction products. *Prog Nucl Energy.* 2016;92: 104–118.
- [65] Porcheron E, Dazon C, Gelain T, et al. Fukushima Daiichi fuel debris retrieval: results of aerosol characterization during laser cutting of non-radioactive corium simulants. *J Nucl Sci Technol.* 2020;58:87–99.
- [66] Green Don W, Perry Robert H. Perry's chemical engineers' handbook. 8th ed. New York: McGraw-Hill companies; 2007. p. 12–29.
- [67] Nakayoshi A, Suzuki S, Okamura N, et al. Prediction of the drying behaviour of debris in Fukushima Daiichi Nuclear Power Station for dry storage. *J Nucl Sci Technol.* 2018;55(10):1119–1129.
- [68] Nakayoshi A, Jegou C, De Windt L, et al. Leaching behavior of prototypical corium samples: a step to understand the interactions between the fuel debris and water at the Fukushima Daiichi reactors. *Nucl Eng Design.* 2020 Apr;360:110522.
- [69] Kirishima A, Nagatomo A, Akiyama D, et al. Study on the chemical structure and actinide leaching of MCCI debris. *J Nucl Mat.* 2019 Sep;527:151795.
- [70] Washiya T, Yano K, Kaji N, et al. Study of treatment scenarios for fuel debris removed from Fukushima Daiichi NPS. Proceedings of the 23rd International Conference on Nuclear Engineering (ICONE 23); 2015 May 17-21; Chiba (Japan). [DVD-ROM].
- [71] Japan Atomic Energy Agency, Analysis of Debris Samples of Tokyo Electric Power Company Holdings Fukushima Daiichi Nuclear Power Station (English translation), JAEA-Review 2020-055, December 2020.
- [72] OECD/NEA. Available from: <https://www.oecd-nea.org/>
- [73] SAREF project report, Available from: <https://www.oecd-nea.org/nsd/docs/2016/csni-r2016-19.pdf>
- [74] PreADES project. Available from: https://www.oecd-nea.org/jcms/pl_25169/preparatory-study-on-analysis-of-fuel-debris-preades-project
- [75] ARC-F project. Available from: https://www.oecd-nea.org/jcms/pl_52958/analysis-of-information-from-reactor-building-and-containment-vessel-and-water-sampling-in-fukushima-daiichi-nps-arc-f-project

- [76] Nakayoshi A, Rempe J, Barrachin M, et al. Review of Fukushima Daiichi Nuclear Power Station debris endstate location in OECD/NEA preparatory study on analysis of fuel debris (PreADES) project. Nucl Eng Design. 2020 Sep;369:110857.
- [77] BSAF project report. Available from: <http://www.oecd-neo.org/nsd/docs/2015/csni-r2015-18.pdf>
- [78] TCOFF project. Available from: https://www.oecd-neo.org/jcms/pl_25584/thermodynamic-characterisation-of-fuel-debris-and-fission-products-based-on-scenario-analysis-of-severe-accident-progression-at-fukushima-daiichi-nuclear-power-station-tcoff
- [79] TCOFF final report (in print). This report will be available in the OECD/NEA site shortly.